Civil Engineering Infrastructures Journal xx,xx
DOI: 10.22059/ceij.2025.383599.2169

Numerical Analysis of Variable Uplift Pressure Distribution on Earthquake-Induced Acceleration Surface at Crack Locations in Concrete Dam Body

Mardookhpour,A.R[1], Mohammadalizadeh,S [2], Marhamati,A.M [2]
[1] Assistant Professor, Civil Engineering Department, Lahijan Branch, Islamic Azad University, Lahijan, Iran
[2] MSc, Civil Engineering Department, Lahijan Branch, Islamic Azad University, Lahijan, Iran

Received: 30/11/2024
Revised: 05/04/2025
Accepted: 30/04/2025

Abstract: This study investigates the impact of uplift pressure, taking into account pore water pressure and its variable distribution, on the nonlinear dynamic response of a concrete gravity dam during near and far-fault earthquakes using a 2D numerical model in Abaqus software. During dam body analysis, crack growth initiated from the dam surface across all three accelerograms, and spread at the geometric failure point. Cracks on both sides of the area between the dam surface and the geometric failure point experienced significant tensile damage. A comparison between dam crest lateral displacements based on three selected accelerograms indicated that the maximum lateral displacement occurred at the Morgan Hill accelerogram at 11 centimeters. Moreover, a comparison of dam crest vertical displacements based on the three selected accelerograms showed that the maximum value was recorded at the Northridge accelerogram at 4 centimeters, while the minimum displacement was found at the Loma Prieta accelerogram at 3 centimeters. Comparison of pore water pressure during the earthquake between the heel and toe of the dam based on three selected accelerograms revealed that the maximum pore water pressure was recorded at Morgan Hill accelerogram at 0.065 megapascals, with the maximum pressure for the other two accelerograms being recorded at approximately 0.064 megapascals. Therefore, pore water pressure variations generally showed notable oscillations with a relatively small amplitude during the earthquake. Future studies are recommended to conduct a 3D analysis for more precise investigations.

Keywords

Concrete Dam, Uplift Pressure, Crack, Landslide, ABAQUS Software.

1. Introduction

The design of concrete dams to withstand applied loads and to control their behavior during operation and under dynamic loads, such as earthquake loads, is one of the most challenging issues in dam engineering. Given the significant importance of concrete dams in controlling surface water and generating hydropower and the high cost of designing and constructing these massive structures, investigations related to their issues have always been prioritized over other conventional engineering structures. Moreover, any flaws or deficiencies in the predicted performance of a dam can lead to irreparable material and human losses. Therefore, a precise evaluation of dam performance, especially its behavior under severe dynamic loads, must be conducted with greater care and supervision (Kalateh & Ghamatloo, 2016).

Unreinforced concrete is inherently susceptible to cracking. According to the Rankine failure criterion, cracking occurs if the maximum principal (tensile) stress at a point in the unreinforced concrete exceeds the tensile strength of the concrete. Concrete dams may experience cracking even under service loads (self-weight and hydrostatic pressure). However, under severe earthquakes, the stresses induced at certain points in the dam body will typically exceed the elastic capacity of the concrete dams, resulting in cracking of the dam section and a reduction in the overall stiffness of the structure. The two primary sources of nonlinear behavior in gravity concrete dams include material nonlinearity (tensile cracking or compressive crushing of concrete) and geometric nonlinearity (sliding and uplifting along cracks in cracked surfaces). To achieve realistic results, any mathematical modeling of such problems must provide the capability to investigate the interaction of the dam with fluid and foundation, considering the effects of surface and subsurface topography, in addition to the ability to simulate each domain. Due to wave diffraction and energy dissipation within the system, the finite element method is suitable for modeling such systems under loading conditions. Consequently, analyzing dam behavior requires accounting for the surrounding conditions, including the reservoir. Appropriate boundary conditions must be defined between the dam and reservoir, facilitating information exchange between these two environments through suitable assumptions and conditions during the analysis. Additionally, the distribution and magnitude of uplift pressure can significantly influence the dam's seismic behavior. The presence of drainage wells affects uplift pressure distribution and can be considered a crucial parameter (Kalateh & Ghamatloo, 2016).

A study compared rotational and fixed smeared crack models for gravity concrete dams subjected to earthquake loads. The analyses were conducted using the finite element method and Fortran programming. Results indicated that each cracking model has relative advantages and disadvantages depending on the specific case (Navaeinia et al., 2013).

A study investigated the wave-structure interaction of dam failure from protective walls using SPH and ALE methods. The study employed the Smoothed Particle Hydrodynamics (SPH) method and

Arbitrary Lagrangian-Eulerian (ALE) formulations to investigate wave-structure interaction (WSI) problems. To this end, an equation of state (EOS) with weak compressibility, particularly the Murnaghan equation of state (Murnaghan EOS), was employed to reduce fluid compressibility and apply appropriate numerical time step constraints using the LS-DYNA software. The numerical results of wave forces applied to the obstacle were validated with high accuracy against experimental data. The SPH method demonstrated a higher agreement with laboratory results compared to the ALE method (Rahmati-Alaei & Rokhy, 2025).

A study has been conducted on the safety of existing dams against seismic loads and how new ones should be designed to resist earthquakes. In this study, the Pine Flat Dam in California, USA, was analyzed under static and dynamic conditions by the ABAQUS software to assess hydrostatic forces and dynamic stresses on the dam by considering flexible foundations. The seismic data from the Taft Lincoln School Tunnel earthquake were applied in the vertical and horizontal components to study the linear and nonlinear dynamic behavior of the gravity concrete dam. The most intriguing observation drawn from the nonlinear analysis was that the maximum initial stress at the heel was considerably reduced while the change concerning the value of minimum principal stress was at a minimum. It also can be seen that the maximum principal stress moved from the base to the neck of the dam. These analysis results aided in improving the design of new dams and assessing the seismic safety of the existing dams (Hussein et al., 2024).

One study focused on the impact of long-period pulses in near-fault ground motions on the structural performance of concrete gravity dams. Three sets of near-fault and far-fault ground motion records with similar values at peak ground acceleration were selected for this study. The selection included Superstition Hills 1987, Loma Prieta 1989, and Northridge 1994 earthquakes. The Sarıyar gravity dam, located on the Sakarya River 120 kilometers northeast of Ankara, was selected as a case study and used to explore the impact of near-fault ground motions on the response of the dam. Linear transient analyses were carried out using the selected ground motion records to assess the structural response of the dam. The obtained dynamic characteristics, maximum displacements, maximum and minimum principal stresses, and maximum and minimum principal strains were then compared with the far-fault ground motion record results that exhibited similar PGAs. It was observed from the results that the displacements were increased for all the ground motions along the dam height. The maximum and minimum principal stresses and strains showed a trend of decrement from the toe of the dam to the top, 3.125 meters above the dam's base. The maximum tensile and compressive stresses and strains were also found to be 3.125 meters above the base of the dam (Altunisik et al., 2019).

The Longtan high concrete dam in China was used as a case study in another research, and the static and dynamic conditions of the dam were analyzed to investigate crack formation using ABAQUS software based on the finite element method. A numerical prediction of crack propagation in gravity concrete dams was presented. Acceleration-time records from the 1976 Koyna earthquake were used to conduct a two-dimensional seismic numerical analysis. The cracking zones and crack growth in the dam's concrete during seismic activity were studied. The analyses located areas of high likelihood of crack formation, and the results indicated that the Longtan Dam was partially unstable under seismic conditions. The results of this research provide valuable guidance for the design and operation of dam systems to ensure their safety and resilience (Ghallab, 2020).

A numerical analysis based on the finite element method was performed to estimate crack growth under static and seismic loads, adequately evaluating crack propagation in gravity concrete dams. A set of reasonable assumptions was used in the study to incorporate several key factors, including water pressure within stress-free cracks, fracture process zone (FPZ), cohesion forces within the FPZ, hydrostatic water pressure, and dam reservoir interaction. A general numerical algorithm was proposed to predict crack growth in gravity concrete dams under static and seismic loading conditions based on a mixed mode I-II crack propagation criterion using the stress intensity factor (SIF). It was found that cracks do not initiate until the reservoir water level exceeds the dam height when a gravity concrete dam is subjected to static loading. Additionally, the water pressure within unstressed cracks had a minor adverse impact on the structural resistance to cracking, while the water pressure within the fracture process zone (FPZ) had no impact on the dam capacity. The analysis of seismic crack propagation showed that water pressure in cracks leads to crack propagation downward at an angle toward the downstream face and a longer crack growth than in the case without internal water pressure (Wang et al., 2022).

In a study Wang et al. to evaluate the influence of initial cracks on seismic crack propagation in gravity concrete dams under strong earthquakes, the extended finite element method (XFEM) was introduced to achieve a rational seismic performance assessment. The results from the proposed model were compared with the results reported in the existing literature to verify the validity of the algorithm. The proposed method was used to analyze a scaled 1:40 model of a gravity dam with an initial crack on its upstream face for this purpose. The results obtained were in good alignment with other numerical methods and model experiments. The effects of initial cracks on crack propagation and the seismic response of the gravity dam were subsequently examined. In addition, the study presented the seismic failure processes and modes of gravity dams with initial cracks, which provides valuable information on the behavior of such structures under seismic loads (Wang et al., 2021).

Seismic evaluation of concrete gravity dams is a critical issue that focuses on predicting cracking and its consequences. As general-purpose finite element software is used more and more, research in this area has shifted to quantifying behavior within an assessment framework. Nonlinear analysis and its connection to dam–foundation–reservoir interaction are still challenging tasks. The analysis results and evaluation framework are highly dependent on the modeling approach. Although progress has been made, this field remains an active area of research because of many unresolved issues regarding quantification and assessment of damage, in particular, compared to other major infrastructure components. Arici and Soysal conducted a comprehensive review of the seismic evaluation of gravity dams in one study and identified existing challenges. Different modeling approaches and methodologies for assessing the damaged condition of gravity dams were compared. The sources of both stochastic and epistemic uncertainties in this domain were highlighted, and practical difficulties and theoretical issues were critically examined. Future research directions were also identified to improve seismic evaluation and address uncertainties to improve damage prediction for concrete gravity dams (Arici & Soysal, 2024).

A study focused on the seismic fragility analysis of the dam-reservoir-layered rock foundation system of the Koyna Dam while accounting for the flexibility of the foundation. The dam was modeled using the Concrete Damage Plasticity (CDP) model for nonlinear material modeling, and the Mohr-Coulomb failure model was used for the foundation. Material flexibility, inertial properties, and damping characteristics were accounted for in the finite element modeling. Ground motions were selected for the seismic analysis using the Conditional Mean Spectrum (CMS) approach. Each ground motion was scaled to various intensity levels and directly used for time history analysis using the Incremental Dynamic Analysis (IDA) method. Peak Ground Acceleration (PGA), Peak Ground Velocity (PGV), and Acceleration Spectrum Intensity (ASI) were selected as intensity measure (IM) parameters. The failure limit state in the fragility analysis was tensile cracking in the dam. Damage indices based on crack length and dissipated energy in the dam were used to develop analytical fragility curves for different damage states of the gravity dam. The numerical results showed that dams built on hard rock layers are safer than those on flexible rock layers and that dams with more flexible rock layers are more sensitive to seismic forces (Tidke & Adhikary, 2021)

Wang et al. conducted a detailed investigation of a 203-meter-high gravity dam under construction in a seismically active region to assess its dynamic responses, damage mechanisms, and safety evaluation. The dynamic characteristics, seismic responses, failure modes, and safety assessment of the structure were studied through dynamic failure testing on a scaled model using a shake table. Due to the low material strength of the model, traditional strain gauges could not be effectively attached to the model's surface, and accurate strain measurements during the test were challenging. Therefore, Fiber Bragg Grating (FBG) strain sensors were employed because of their high sensitivity, allowing precise strain measurements in the scaled model during testing. Both dynamic and residual strains were captured using the embedded FBG sensors. During the test, the model was subjected to seismic waves from the Chinese seismic code. Results demonstrated that the proposed embedded FBG sensor provided accurate strain data and overcame the limitations of traditional strain gauges. Based on the fundamental frequency responses and accelerations recorded during the test, the dam sustained damage under seismic waves with a Peak Ground Acceleration (PGA) of 0.3458g. This finding was corroborated by the damage process and strain responses observed during the test. The PGA that caused the first crack in the concrete dam was identified as a critical parameter for evaluating dam safety under strong earthquakes. For this model, the initial cracking occurred at a PGA of 0.3458g, approximately 1.378 times the designed seismic acceleration. Complete failure of the model occurred at a PGA of 1.4176g, demonstrating the dam's capacity to withstand seismic forces up to 5.65 times the designed load. These results indicate that the 203-meter-high concrete gravity dam can be considered safe under severe earthquakes in its location (Wang et al., 2019).

Crack monitoring is required during the construction of new dams to ensure the reliability of existing structures. Precise evaluation of the concrete dam performances is required to predict current and future cracks and to assess seismic capacity. The ability of the upstream and downstream walls of concrete dams to withstand seismic movements is analyzed based on the motion of the upstream and downstream walls. The Koyna Dam was selected as a case study in research as it is relevant to dam foundation interactions in the study of seismic instabilities. The research focused on the dam reservoir foundation interaction with crack and crack propagation effects. Regions where tensile stresses exceeded the allowable limit were assumed to form cracks. Crack was modeled using the Extended Finite Element Method (XFEM). Seismic stress analysis of the Koyna Dam revealed the following regions have high tensile stresses exceeding the tensile strength of concrete: at elevations of 55 and 85 meters above the base on the reservoir side at the point of slope change, the dam base, and the downstream neck of the dam. The Koyna Dam was examined for various initial crack conditions. The influence of initial crack positions on crack propagation mechanisms induced by seismic responses was thoroughly analyzed (Parvathi et al., 2022).

A study was done to see how dam body saturation affects seismic performance, as concrete saturation can change its properties and how it behaves under different loads. For their case study, Ghanioun et al. chose the Koyna concrete gravity dam. They initially determined the properties of saturated concrete, including the modulus of elasticity, compressive and tensile stresses, and compressive and tensile strains. They mapped the boundary between saturated and unsaturated areas using the ABAQUS software, using three reservoir water levels. They used an Eulerian-Lagrangian approach to capture both structural and fluid dynamics for seismic modeling. For far field and near field conditions, they simulated earthquakes of varying frequencies scaled to a max acceleration of 0.5g. Results indicated that saturation altered the fundamental frequencies of the dam and had a significant effect on its behavior. Saturation usually reduces maximum displacements under linear conditions. In nonlinear cases, saturated conditions often result in less structural damage, especially in dams with shallow reservoirs.

Another study by Feng et al. compared stress and displacement patterns in conventional concrete gravity dams with more flexible ones. They used finite element analysis to find that as dam height decreases, stress increases and vertical displacement decreases during regular operations in both dam types. However, maximum stress under earthquakes was four times higher than in operational periods and was observed in the weakest points of the dam. Interestingly, flexible dams consistently had higher stress and displacement than traditional concrete dams across all conditions (Fang, et al., 2024).

Dams are massive structures capable of storing large quantities of water, and the failure of a dam places many people at considerable risk of loss of life. A complex but critical part of dam safety parameters is studying their response to static loads. Over its static response, evaluating concrete gravity dams, one of the key soil-structure interactions (SSI) is considered. The static behavior of the Bakra dam was analyzed using the finite element software ANSYS in one study. Stress distribution within the dam is critically dependent on the interaction between the foundation structure and the reservoir water level. Separately, dams with rigid, mass, and non-mass foundations were developed into various 2D models. The importance of foundation flexibility was evaluated by varying the ratio of dam-foundation rock interactions. Different dam foundation rock interaction ratios were examined to determine the significance of foundation flexibility. The importance of foundation structure interaction was demonstrated by combining foundation mass and stiffness and analyzing their effect on the dam's static response in terms of deformation and stress distribution. The maximum deformation in the dam was observed at the crest, with displacements of 567 mm for the mass foundation and 617 mm for the non-mass foundation. These values were greater compared to 527 mm for the rigid foundation. The proposed finite element method (FEM) model can also be used for dynamic analysis, including foundation dam and fluid dam interactions (Sharma & Nallasivam, 2023).

The seismic response of a concrete gravity dam was analyzed through a numerical study. The finite element method with pre-implemented discontinuities was used as the numerical method. An explicit time-stepping approach was used to solve the equation of motion, including boundary conditions of ground motion excitation, static structural weight, hydrostatic reservoir load, and hydrodynamic reservoir forces. Mass-dependent damping was used instead of stiffness-dependent damping, as the latter does not lead to a significant reduction of the critical time step during explicit temporal integration. As a numerical example, the Koyna Dam was analyzed using actual acceleration records from the 1967 earthquake. The simulation results were found to correlate strongly with previous studies, especially in predicting crack propagation within the dam body. This approach offers a robust approach to understanding the seismic vulnerability of gravity dams (Saksala & Mäkinen, 2020).

Gravity dams are a critical infrastructure for water storage, flood control, and energy generation. Protection of lives, property, and the environment from the catastrophic consequences of dam failure requires ensuring that dams will remain structurally intact under seismic loads. The seismic response of a concrete gravity dam under earthquake and hydrostatic forces was analyzed by Tuswan et al. using ABAQUS software, and the results were validated against experimental data from Tao et al. Four key variables were considered in the analysis, namely mesh size, dam slope, dam width, and the peak acceleration of the Koyna earthquake in Mumbai, India, to compare the dam's response under seismic loads. The results indicated that the dam slope can be increased to reduce stress in the neck region of the dam. But a steeper slope in the neck area could be a problem, as it shifts stress to the dam's lower parts. In addition, the width of the dam structure can be adjusted to reduce stress in its lower sections. However, increasing the width shifts tensile damage tendencies towards the upstream face of the dam, which is undesirable. An increased risk of dam vulnerability and dam failure during an earthquake is highlighted (Tuswan et al., 2024).

In an innovative two-dimensional dam reservoir foundation analysis using finite element modeling in ABAQUS software, Hajivand Dastgerdi, and colleagues systematically investigated the seismic damage mechanisms of the Koyna dam, particularly the upstream angle variations and cross-sectional modifications during earthquake loading. The research methodology consisted of developing an initial model to validate the Koyna dam failure mechanism, followed by strategic geometric transformations and viscous damper boundaries to greatly speed up model generation in ABAQUS compared to traditional infinite element approaches. The researchers used advanced numerical simulation techniques and found that trapezoidal-shaped dams with carefully designed upstream angles were much less structurally damaged than other geometrical configurations. As a result, the study suggested critical design recommendations for concrete gravity dams, which include the strategic use of downstream water forces through upstream angle optimization to mitigate heel region vulnerabilities and minimize abrupt cross-sectional changes to improve overall seismic resilience and structural integrity under dynamic loading conditions (Hajivand et. al., 2022).

Machelski and Korusiewicz investigated the contact interaction between corrugated steel shells and soil based on measured deformations of the shells. Two algorithms were developed to analyze the results. The first algorithm determined the internal forces in the shell based on unit strains, subsequently calculating the contact interactions. This method requires many distributed measurement points around the shell's circumference. In the second algorithm, compatibility conditions were employed, requiring the results obtained from the shell geometry model to align with the measured displacements at the structure's compatibility points. The accuracy of the estimated results improves as the number of points increases. As an advantage, both algorithms take the physical properties of the backfill soil layers into account, but more importantly, they account for the effects of layering and compaction. The results of such analyses can serve as a benchmark for comparing the performance of conventional geotechnical models (Machelski & Korusiewicz, 2021)

Pundrik et al. studied the seismic behavior of a gravity concrete dam subjected to near-fault and far-fault ground motions, considering the dam-reservoir-foundation interaction. Eight different earthquake ground motion records were considered for time-history analysis. The seismic performance of the dam was evaluated using the Cumulative Overstress Duration (COD) and capacity-demand ratio (CDR). The results highlighted the significant impact of near-fault ground motions on the seismic performance of gravity concrete dams (Pundrik et al., 2020).

Gorai and Maity conducted a comprehensive study to investigate the seismic behavior of dams subjected to near-fault and far-fault ground motions, with a focus on seismic safety assessment. They also explained in detail existing modeling techniques for dam-reservoir-foundation systems, failure modes, seismic analysis methods, and the seismic response of various dam types to near-fault and far-fault earthquakes. Finally, they aimed to identify research gaps that need to be addressed (Gorai and Maity, 2021).

A study investigated a non-destructive testing (NDT) method for crack detection using a two-stage convolutional neural network (CNN) model that combined AlexNet and YOLO models using transfer learning. The developed model was precisely tested within simulated environments and through physical experiments using a UAV (unmanned aerial vehicle) to evaluate its effectiveness. A two-stage model based on AlexNet and YOLO was developed for crack classification and segmentation, which utilized transfer learning to address the limitations of traditional CNN models. A well-known dataset was employed to evaluate the developed model in order to compare its performance with other models. The classification network achieved an accuracy of over 90%, while the segmentation network successfully identified and mapped cracks in 85.71% of images. Finally, the developed model was implemented using a UAV within a controlled environment to perform crack detection and segmentation. These findings confirmed that the model is able to detect and categorize structural cracks, highlighting its potential as a reliable tool for enhancing the maintenance and safety of architectural structures (Sorilla et al., 2024).

A study investigated the impact of failure parameters and their progression curves on the outflow hydrograph and presented two approaches: 1. Creating new equations for the average breach width and its formation time using global dam failure data and regression analysis. 2. Applying said equations in a two-dimensional dam failure modeling using HEC-RAS software and comparing them with recommendations in technical literature. The results of the extracted equations were similar to those of the technical literature. This study introduced an innovative aspect by examining the mutual interaction of results and flood zones on the outflow hydrograph, offering a comprehensive perspective on dam failure dynamics and its hydraulic consequences (Praštalo et al., 2024).

The current study investigates the vulnerability and damage of gravity concrete dams subjected to far-fault and near-fault ground motions, considering variable uplift pressure distributions at the earthquake location and the dam-reservoir-foundation interaction. The novelty of this study lies in investigating the impact of variable uplift pressure distributions and their nonlinearity on crack initiation, propagation, and the associated modeling.

The current study employed the article by Kalateh & Ghamatloo (2018) for validation due to its similarity of content and identical case study (Shafarud Dam). Kalateh & Ghamatloo (2018) applied the uplift force as a fixed trapezoidal load. In order to differentiate the present study, pore water pressure was accounted for as a variable, and the uplift force was calculated and applied at each moment in ABAQUS software based on the finite element method. Comparisons were made with the study by Kalateh & Ghamatloo (2018) when necessary for verification purposes. In addition to dam body displacement, cracks in the dam body were also precisely examined two-dimensionally (due to the absence of complex calculations) using selected accelerograms.

2. Materials and Methodology

Crack types, locations, and causes within dams are determined by the analysis of forces acting upon dams, particularly their distribution and safety factors and allowed stresses. These studies are particularly important in concrete dams, which are subjected to water pressure, possible settlements, and even seismic forces. The analysis of concrete dams is aimed at determining the magnitude and distribution of stresses in the dam body and foundation to verify the dam stability factors and to ensure the reliable design of a concrete dam and its ability to withstand applied loads. These analyses are of great help in identifying the weak points and damaged sections of the dam structure and preventing cracking and its subsequent damage to all dam components.

3. Equations Governing the System

The governing equations can be solved using the explicit and implicit methods, with the main difference being observed in stability and efficiency. Conditionally stable explicit methods have a limit on the time step (Δt) that can be used. Therefore, they need a large number of time steps. However, implicit methods are usually unconditionally stable, meaning that stability does not depend on a change in Δt. The explicit method in the direct integration method has lower problem-solving costs and more steps, while the implicit method has higher problem-solving costs and fewer steps. In explicit methods, however, the solution is pushed step by step from the boundary with smaller matrices, which can even be solved manually. This method converges after many errors and iterations, has higher error rates than the implicit method, and takes a lot of time to reach the final result. Since the system of equations is small and is solved in multiple stages, no high-performance processor is required. The explicit method in ABAQUS software does not allow the user to manually determine the growth rate of nonlinear problems. The growth rate is instead calculated automatically at each stage according to stability conditions. The governing system of equations for the entire mesh is solved simultaneously in the implicit method, and the entire mesh is discretized. This results in fewer iterations to converge the finite element equations governing the entire system. As a result, if an error is introduced in each iteration, the solution obtained has less accumulated error than the explicit method because of the fewer iterations. Nevertheless, since this method involves solving a large coefficient matrix, it is not suitable for large-scale problems, e.g. problems with many elements or high complexity, as it requires a powerful processor (Akkas et al., 1979).

3.1 Concrete Damage Plasticity (CDP) Model

Assuming a linear behavior in seismic response analysis of gravity concrete dams does not typically lead to satisfactory results. The accuracy of the results from nonlinear analysis depends on the method utilized in modeling the concrete materials composing the dam body. Numerous behavior models aimed at explaining the complicated mechanical behavior of concrete materials under seismic loads have been developed. This section focuses on the basic behavioral model developed by (Lubliner et al., 1989), which was later modified by (Lee et al., 1998). This model accurately captures the nonlinear behavior of each component in multi-phase composite materials, leading to its widespread use in simulating seismic cracking of concrete dams. The uniaxial strength in this model is composed of two distinct stiffness degradation and plasticity sections to account for permanent deformations. This model generally assumes two primary failure mechanisms in concrete materials, namely tensile cracking and compressive stress-induced crushing. The Concrete Damage Plasticity (CDP) model in ABAQUS software was selected and employed in modeling to investigate the nonlinear dynamic behavior of concrete. The input parameters in a CDP model can be divided into three main categories. The first category of input parameters defines the range of elastic behavior within concrete materials under initial loading up to the elastic threshold. The first section is comprised of two main parameters: Elastic Modulus and Poisson's Ratio. The second category of input parameters is necessary for modeling the plastic (nonlinear) behavior of concrete and is used to create the plastic potential and failure functions. The third category of input parameters determines the stiffness degradation process of concrete materials under the loading cycle.

3.2 Solving Reservoir's Equation

In 1933, Westergaard (Westergaard, 1933) was the first to solve the wave equation for rigid dams during earthquakes. In his solution, the reservoir extended infinitely upstream, and the effects of surface waves were neglected. The fluid was assumed to have a small amplitude and be inviscid. He demonstrated that, under these conditions, hydrodynamic waves could be represented as a specific finite mass of fluid moving with the dam. This is known as the added mass method. Consequently, to account for the reservoir's effects, it suffices to attach a portion of the fluid mass to the dam body and assume it moves with the dam. For water with a unit weight of 9810 N/m³, the width of water oscillating horizontally with the dam can be determined using Eq. (1) (Gorai & Maity, 2021).

$$b=\frac{7}{8}\sqrt{h(h-y)} \tag{1}$$

3.2 Defining an Acoustic Environment for the Reservoir

The governing equation for finite amplitude motion of a compressible, inviscid fluid flowing through a porous, resistant matrix material is given by:

$$\frac{\partial p}{\partial x}+\gamma u^{f}+\rho_{f}\ddot{u}^{f}=0 \tag{2}$$

Where p is the dynamic pressure of the fluid (excluding initial static pressures), x is the spatial position of the fluid particle, u^f is the velocity of the fluid particle, $\ddot{u}^f$ is the acceleration of the fluid particle, and γ is bulk viscosity. The bulk viscosity causes the dissipation of acoustic wave energy. Here, the fluid is assumed to be compressible and inviscid, such that the bulk modulus of the acoustic medium relates the dynamic pressure of the medium (P) to the volumetric strain (ε_V) through the following equation (Sherong, 2013):

$$P=-K_{f}\varepsilon_{V} \tag{3}$$

where $\varepsilon_V=\varepsilon_{11}+\varepsilon_{22}+\varepsilon_{33}$. Therefore, both the bulk modulus K_f and the density ρ_f of the acoustic medium must be defined. Acoustic analysis is employed to model sound propagation, which can also include waves impinging on a structure. This type of analysis is only effective in dynamic simulations and can be used to model coupled structure-acoustic systems. Moreover, acoustic elements must be utilized, and in the analysis of coupled structure-acoustic systems, the interaction between the structure and the acoustic medium should be modeled based on surface coupling using tie constraints or, in the ABAQUS standard, using acoustic interface elements (Yang & Zhou, 2015).

3.3. Solution for the Governing Equations

The structural response will also be time-dependent when the structure loading is time-dependent. Calculations indicate that if the loading frequency is less than one-quarter of the structure's natural vibration frequency, the structural response will barely exceed the static response, and therefore, quasi-static methods can be employed. However, dynamic analysis will be required if the loading frequency is higher or is applied suddenly to the structure. In dynamic analysis, in addition to the stiffness matrix, the mass and damping matrices are also necessary (Yang & Zhou, 2015).

In dynamic analysis, the transient response, often referred to as the response history, is sought. This requires the time integration of the equation of motion. Direct integration is a time-stepping method where the structural response is calculated at intervals of Δt. At the nth time step, the equations of motion can be expressed as follows (Sherong, 2013):

$$M\ddot{u}_n+C\dot{u}_n+R_n^{int}=R_n^{ext} \tag{4}$$

$$M\ddot{u}_n+C\dot{u}_n+Ku_n=R_n^{ext} \tag{5}$$

Where M is the mass matrix, C is the damping matrix, K is the stiffness matrix, R_n^{int}, and R_n^{ext} are the internal and external force matrices, respectively, and u_n is the nodal displacement matrix of the structure (Sherong, 2013). Equation 4 is applicable for linear and non-linear systems, while equation 5 is only applicable for linear systems. If the system is non-linear, R_n^{int} includes non-linear effects, thus making equation 4 the more general option.

4. Case Study

The subject of this research is the Shafarud Dam constructed on the Shafarud river. The dam is located on the outskirts of Rezvanshahr, Gilan Province. Figures 1 and 2 depict the dam's geometry and the concrete dam with its foundation and reservoir, respectively.

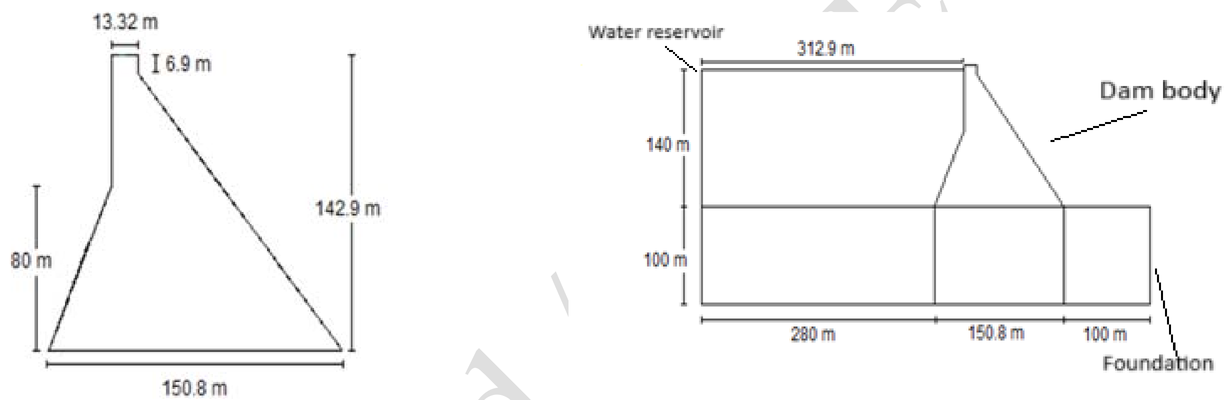

(a) (b)

Figure 1. Schematics of Shafarud Dam: (a) geometry of the dam and (b) geometry of the dam, foundation, and reservoir

5. Preliminary Concepts in ABAQUS Software

5.1 Introduction to ABAQUS Software

ABAQUS Software is a set of engineering simulation programs based on the finite element method (FEM) and is able to solve a wide range of engineering problems, from simple linear simulations to complex nonlinear ones. ABAQUS includes an extensive library of elements and materials, allowing it to model nearly all common engineering materials. Additionally, this software is able to perform structural analyses, including stress displacement, thermal, electrical, soil mechanics, and mass transfer, as well as interaction analyses, such as fluid-structure interaction. In nonlinear analyses, ABAQUS automatically selects and continuously adjusts the appropriate loading sample during the analysis to determine the accurate answer efficiently.

ABAQUS is comprised of two main analysis processes:

- ABAQUS /Standard
- ABAQUS /Explicit

ABAQUS /Standard is a general analytical process able to solve a wide range of linear, nonlinear, static, and dynamic analyses. This process analyzes the governing system of equations at each interval using implicit methods. Conversely, ABAQUS /Explicit advances the analysis through time using time intervals without solving the system of equations at each step. Modeling in ABAQUS is done through using methods, with the most accessible method being the employment of the complete graphical interface within ABAQUS. This user-friendly interface simplifies tasks such as creating various models, defining differing materials, loads, and boundary conditions, performing meshing, determining element types, and reviewing analysis results (Sherong, 2013).

5.2 Working with ABAQUS

5.2.1 Finite Element Method (FEM)

The finite element method is a modern numerical analysis technique that was initially used in structural engineering. This method is able to solve different problems in various disciplines, particularly in continuum mechanics. FEM was initially developed in the mid-20th century across two different approaches in engineering and mathematics. Simple bar structures calculated based on familiar static methods replaced the Complex spatial structures in engineering calculations.

During the last decade, FEM and its utilization have advanced and evolved significantly in nonlinear continuum mechanics, manifesting in geometrical nonlinearity, material behavior, structural dynamics, fluid dynamics, Structural optimization, etc. (Sherong, 2013).

5.2.2 Modeling Nonlinear Concrete Behavior in ABAQUS

ABAQUS software includes various structural models for analyzing the nonlinear behavior and cracking of concrete materials under low confining pressure. These models depend on the specific product selected for analysis. The Concrete Craze Cracking Model is available in ABAQUS /Standard, the Concrete Brittle Cracking Model is available in ABAQUS /Explicit, while the Concrete Damaged Plasticity Model can be utilized in both ABAQUS /Standard and ABAQUS /Explicit. The Concrete Damaged Plasticity (CDP) Model in ABAQUS can model concrete and other semi-brittle materials of all structural types, including beams, shells, and solids. This model consists of a combination of non-associated multi-hardening plasticity and scalar damage elasticity to describe the permanent damage occurring during failure processes, which allows the user to control stiffness recovery during load reversal cycles and can also be defined as sensitive to strain rate variations.

5.3 ABAQUS Modeling

This section delves into modeling within the ABAQUS software and subsequent verification. Initially, the model presented in the reference article is modeled and verified. The Shafarud Dam in Gilan, Iran, serves as the model for verification. After ensuring the accuracy of the modeling and analysis, the impact of the variable uplift pressure distribution at the earthquake-induced acceleration level at the concrete dam's crack location is assessed, and finally, the results are compared. The elements are modeled as two-dimensional shell elements. Regarding element type selection, the concrete dam elements are defined as plane strain, the soil elements as coupled stress-pore water, and the water elements as acoustic.

It is necessary to have realistic pore water pressure in the soil to account for the variable uplift pressure at the level of earthquake-induced acceleration. This ensures that during seismic acceleration, the changes in pore water pressure accurately determine the resulting uplift force, and the pore water pressure is not applied as an independent, manually exerted load. To this end, a three-step analysis is conducted. In the first step, geostatic forces are stabilized and applied to the saturated soil. Subsequently, the concrete dam and water reservoir loads are transferred to the soil, and consolidation occurs. During this process, the pore water pressure in the soil beneath the dam stabilizes. During the earthquake step, the stabilized pressure is applied.

First, different model components are built, and the dam, reservoir, and concrete lining cross-sections are drawn in 2D software and then converted into 3D elements.

Given that this study employed a two-dimensional analysis, the following points should be noted:

- Fluid movement behind the dam is a three-dimensional phenomenon, including surface waves and wave effects moving along the dam length, which are not well-captured in a 2D model.
- Reflected waves and complex fluid flows behind the dam are better modeled in a 3D analysis.
- Water flow may cause localized erosion at different dam points, which is not well-simulated in a 2D model.
- In a 2D model, crack interaction with earthquake motion is examined only in a specific plane, and complex crack variations along the dam are ignored. In a 3D model, crack propagation along the length of the dam can be examined, thus contributing to a more realistic modeling.

- Regarding uplift, lateral forces are accounted for across the entire dam volume in a 3D model, potentially presenting a more realistic pressure distribution.

- 2D analysis is simpler, requires simpler calculations, and can provide acceptable results if modeling is performed under optimal conditions. These characteristics are the primary reasons for conducting this study in a 2D format.

6. Material Specifications

The material properties of the concrete were defined based on the concrete used in the study by Kalateh and Ghamatloo (Kalateh & Ghamatloo, 2018). In addition to elastic properties, concrete's plastic and failure characteristics were fully incorporated. Furthermore, the water properties were defined as an acoustic element. Determining concrete properties solely based on an elastoplastic diagram is quite difficult. One of the most critical parameters needed for accurately defining concrete behavior is concrete damage plasticity (CDP), which can be obtained through cyclic loading and unloading tests on cubic specimens in the laboratory. Table 1 shows the properties of the concrete used.

Table 1. Concrete properties

Critical crack opening (mm)	**Tensile strength (MPa)**	**Ultimate strain (%)**	**Peak strain (%)**	**viscosity**	**Bulk modulus**	**f_{b0}/f_{c0}**	**Centrifugal effect**	**Density (kg/m^3)**	**Poisson's ratio**	**Young's modulus (GPa)**	**Yield stress (MPa)**
0.156	3	0.35	0.275	0.0001	0.667	1.16	0.1	2630	0.2	30	25

7. Analysis Steps

In order to account for the variable uplift impact at the accelerogram application level, actual pore water pressure must exist in the soil. The pore water pressure variations determine the actual magnitude of uplift force during earthquake acceleration application, while the uplift pressure is not manually entered as an independent load. The analysis is conducted in four steps. The initial step establishes the initial conditions. A nonlinear explicit dynamic analysis is performed, with the analysis duration matching the selected acceleration time history. The second step involves geostatic analysis to stabilize the initial soil conditions and geostatic loads. The third step, soil, consolidates the saturation percentage, porosity, pore water pressure, and gravity loads of the dam and reservoir over 7200 seconds. In the final step, a nonlinear dynamic analysis is performed, applying the acceleration time histories with their characteristic time.

7.1 Interactions

The dam and foundation are discretized for the analysis using linear plane stress, 4-node, reduced integration solid elements (CPS4R). The reservoir is modeled as 2D linear acoustic elements (AC2D4).

Tie constraints are employed to model the interaction between the components (i.e., concrete dam, foundation, and water). A frictionless contact is assumed between the dam and water at the foundation interface.

In the initial geostatic analysis, the dam and reservoir are inactive. They are added and activated in the subsequent soil step, first as inactive and then activated in a subsequent sub-step.

7.2 Boundary Conditions

The boundary conditions were defined to fix the foundation base and the sides for the first and second analysis steps. Moreover, the vertical constraint of the foundation during the earthquake application, along with the application of the acceleration time history, was applied in the third analysis step.

7.3 Accelerogram Selection

The model analysis employed three accelerogram histories: Morgan Hill, Loma Prieta, and Northridge. These time histories were scaled to 0.35g using the SeismoSignal software (Retrieved from http://ngawest2.berkeley.edu).

Due to forward directivity and permanent ground displacement, ground motions recorded near the fault exhibit distinct characteristics compared to those recorded far from the fault. These characteristics include long-period pulses in time history, acceleration, velocity, displacement, a small ratio of peak acceleration to peak velocity, and a short duration in the fault-normal component.

Other characteristics of these accelerograms, which were of great importance in their selection are as follows (Toppozada et al., 1988; Eguchi et al., 1998; Bruce, 2003):

Significant Magnitude and Intensity:

- Loma Prieta: 6.9 Mw
- Northridge: 6.7 Mw
- Morgan Hill: 6.2 Mw

Extensive and Diverse Impact on Structures

- Northridge: Strong vertical component
- Loma Prieta: Lateral spread impact

- Morgan Hill: Analysis of strike-slip fault behavior and crack propagation in dams and embankments

Spectral and Seismic Response Diversity:

The three earthquakes demonstrated distinct response spectra, which are used as notable input earthquakes in seismic hazard analysis, structure performance evaluation, and seismic design studies.

Given that the accelerogram histories have been pre-scaled, no additional scaling factor was required in ABAQUS. Consequently, the acceleration coefficient was assigned a value of 1. Figure 2 illustrates the accelerogram histories for the Loma Prieta, Northridge, and Morgan Hill earthquakes.

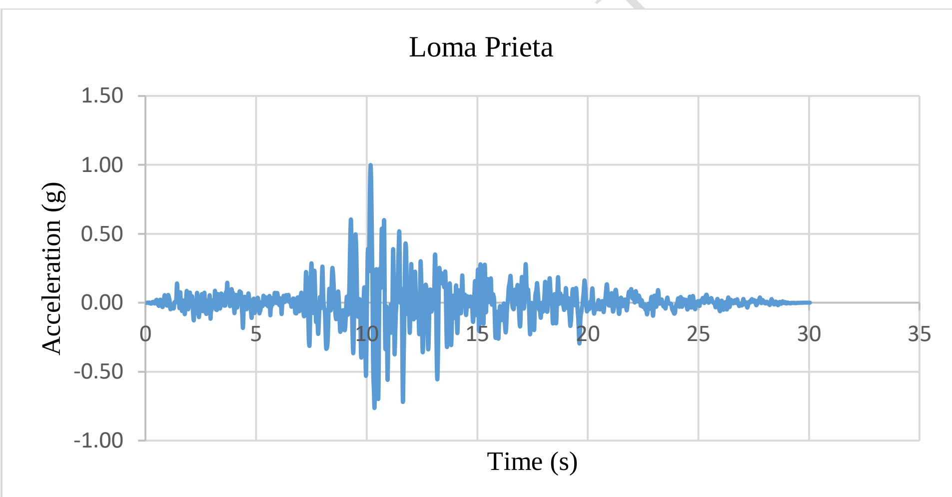

(a)

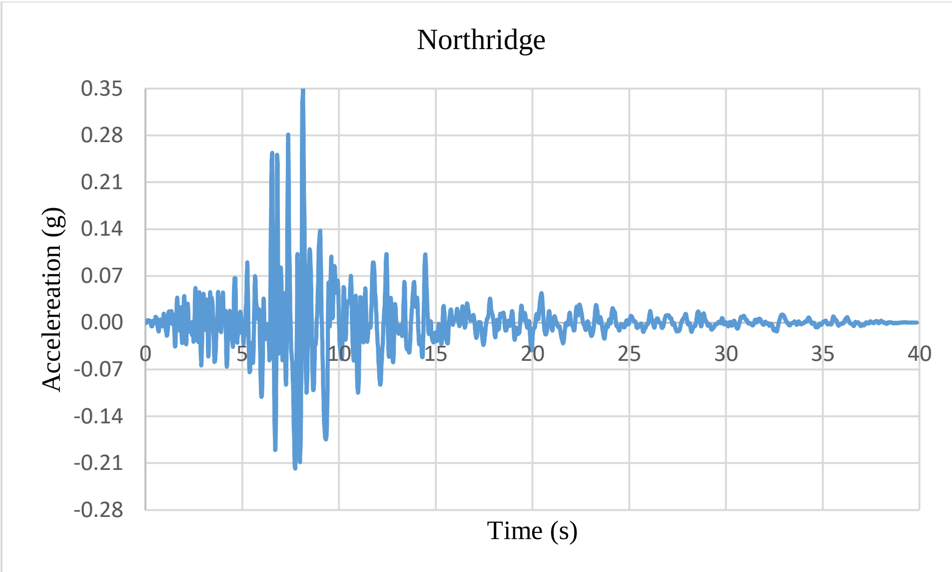

(b)

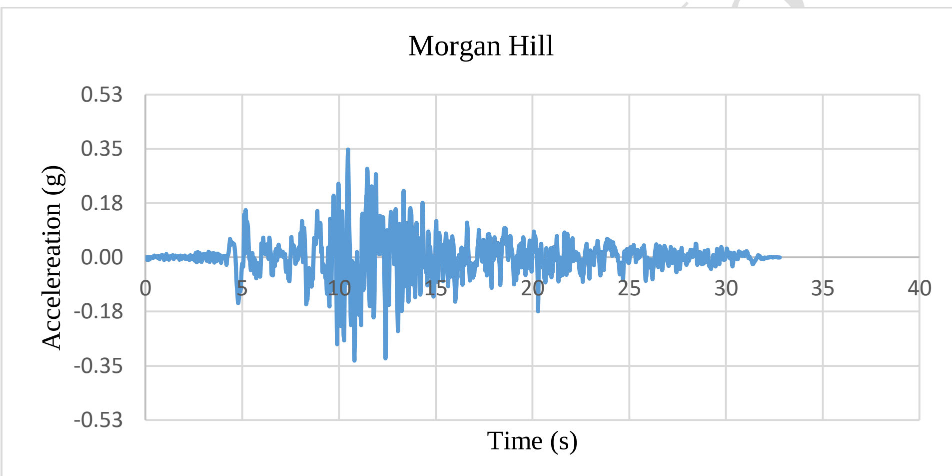

(c)

Figure 2. Accelerogram history of (a) Loma Prieta, (b) Northridge, and (c) Morgan Hill

Each ground motion was input into ABAQUS as an accelerogram history and applied individually to the base of the model via boundary conditions. The effective duration of the ground motion can be employed to expedite the analysis.

Point 1 was assigned an elevation of zero as the top layer of the soil, and Point 2 was assigned an elevation of -100 meters. The geostatic load at Point 2 was determined by multiplying the soil height by the saturated unit weight of the soil. The lateral earth pressure coefficient for the dam foundation was taken as 0.48, which can be rounded to 0.5.

8. Results Analysis

8.1 Verification Analysis Results

The uplift pressure obtained from a previous study (Kalateh & Ghamatloo, 2018) was employed for verification purposes. Figure 3 shows the displacement of the dam's crest (Kalateh & Ghamatloo, 2018), in which blue rectangles represent the case where the uplift pressure is absent.

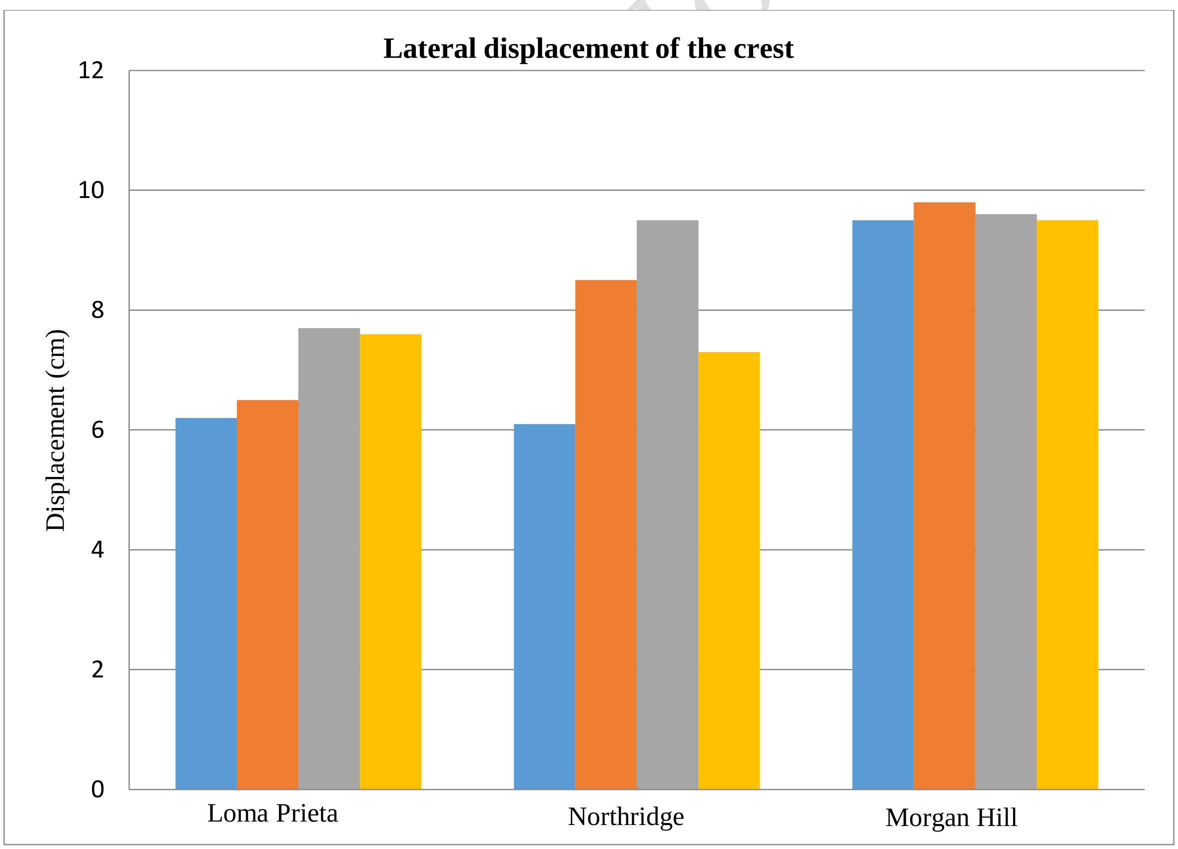

Figure 3. Lateral displacement of the crest (Kalateh & Ghamatloo, 2018)

8.2 Meshing

A method of evaluating the suitability of element dimensions in FEM is examining the results obtained from the element analysis within the model. The observation of significant discontinuities and jumps within the elements in the analysis results indicates insufficient analysis accuracy. Following the conclusion of the simulation, it is essential to thoroughly examine the results from each element to ensure the continuity and convergence of the results, as well as to the adequacy and quality of the dimensions. Three mesh types were used in this study: A simple strain element for the concrete dam, a coupled stress-pore water element for the foundation, and an acoustic element for the reservoir water.

Table 2 reveals a negligible difference between the results of the present study and those of (Kalateh & Ghamatloo, 2018), confirming the validity of the modeling and analysis techniques employed in this research.

Table 2. Comparison of lateral displacement of the crest between the current study and (Kalateh & Ghamatloo, 2018).

Acceleration time history	Lateral displacement of the crest (cm)	
	Kalateh and Ghamatloo, 2018	Current study
Loma Prieta	6.2	6.22
Northridge	6.1	6.08
Morgan Hill	9.2	9.16

8.3 Geostatic Step Analysis Results

Figure 4 shows the stress contours obtained from the geostatic analysis, in which the soil static loads were applied. The maximum stress, which is 1 MPa, is concentrated under the foundation. The displacement contours in Figure 5 show that the geostatic load induced very small displacements.

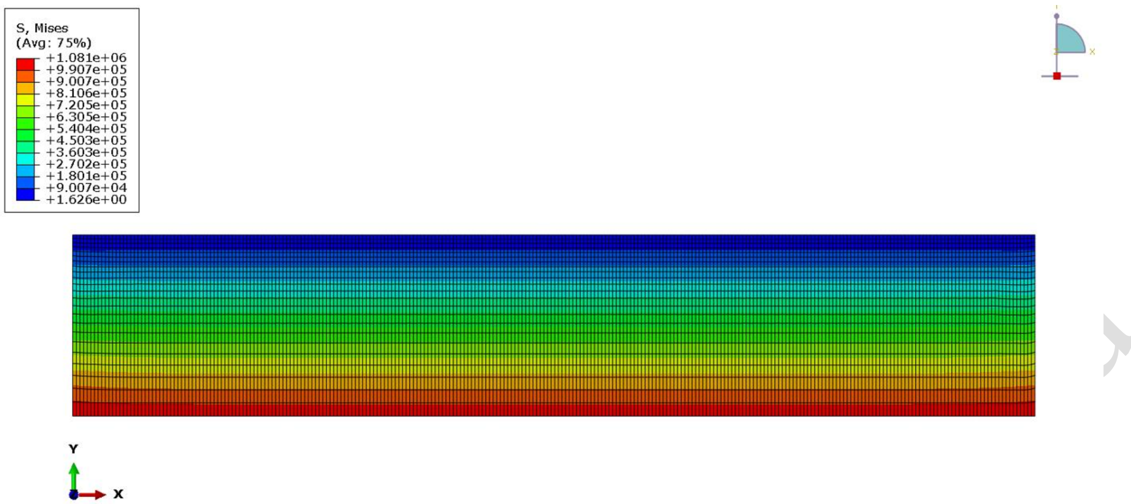

Figure 4. Stress contour for the geostatic analysis step

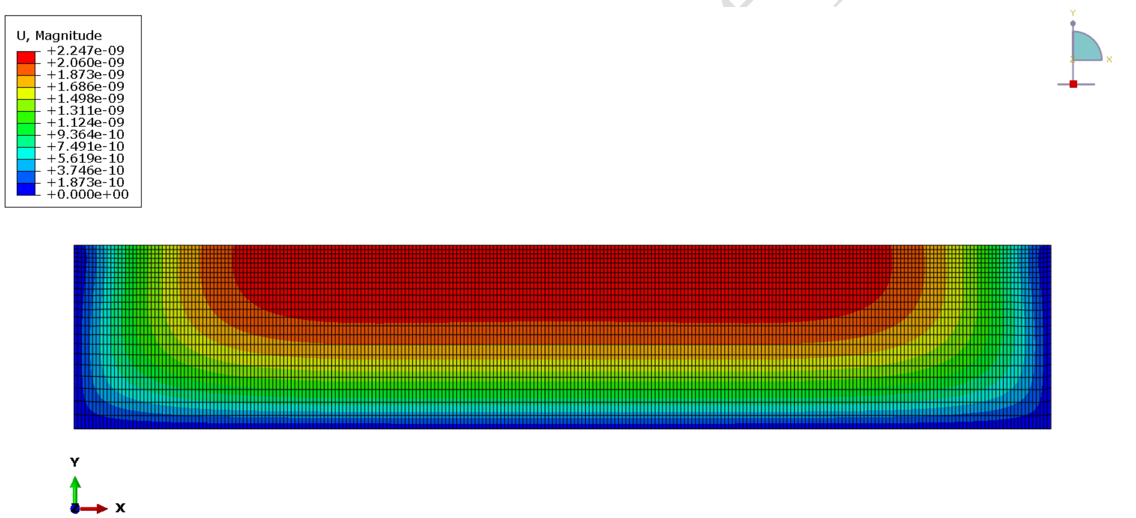

Figure 5. Displacement contour for the geostatic analysis step

8.4 Soil Step Analysis Results

At this step, following the analysis of soil, stress contour, water pressure, displacement, pore water pressure, and water pressure contour at the midpoint of the step, seismic analysis with the following details were presented. Figure 6(a), depicting the stress contour chart during the soil analysis step, indicates that the maximum stress at this step is 2.48 MPa. Figure 6(b), depicting the water pressure contour chart during the soil analysis step, indicates that the maximum stress at this step is 0.059 MPa. This pressure occurs beneath the concrete dam and is attributed to the self-weight of the dam structure. Figure 6(b), depicting the water pressure contour chart during the soil analysis step, indicates that the maximum pressure during this is 0.059 MPa

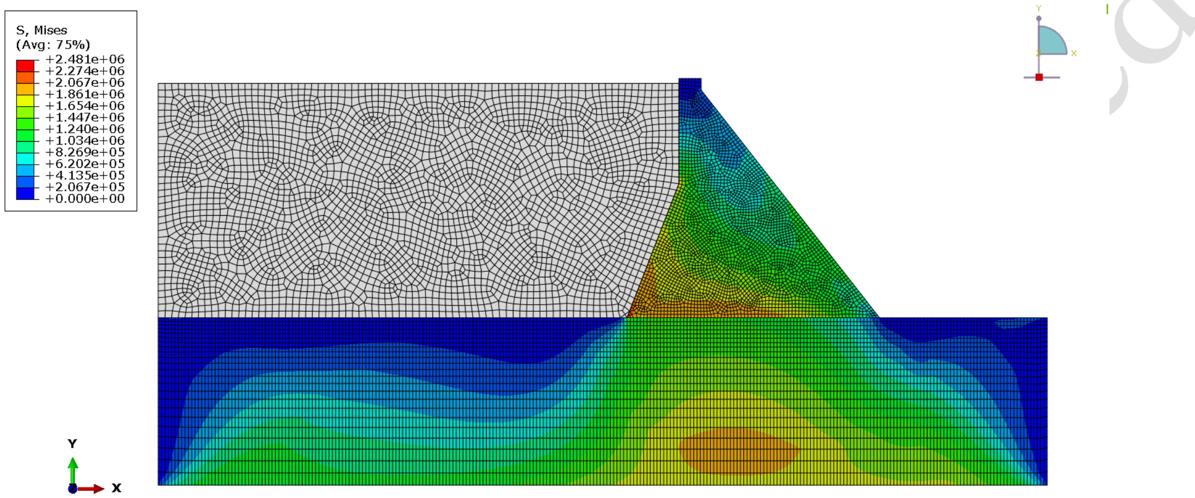

(a)

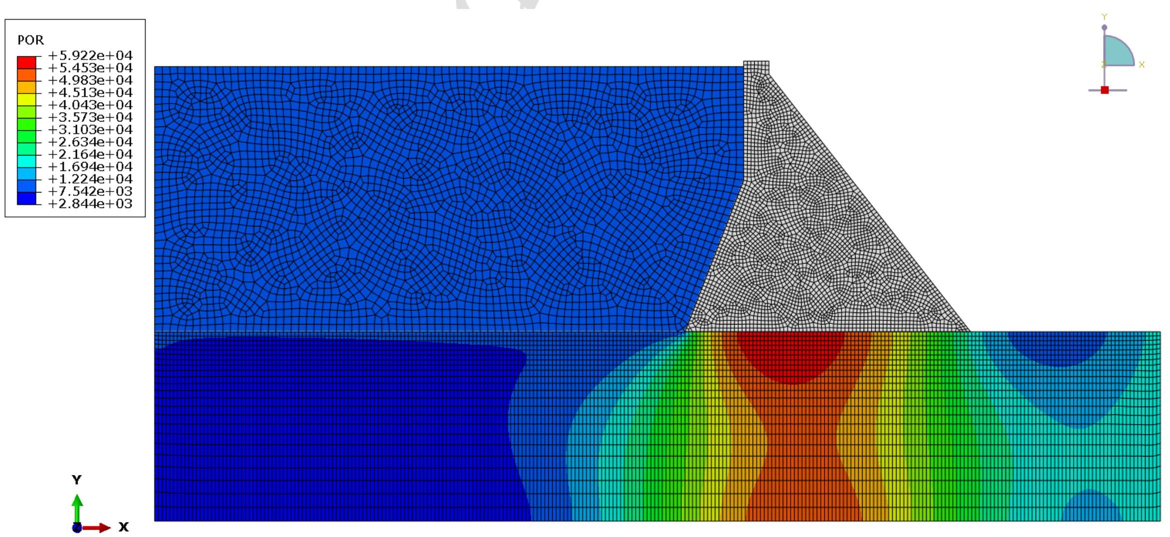

(b)

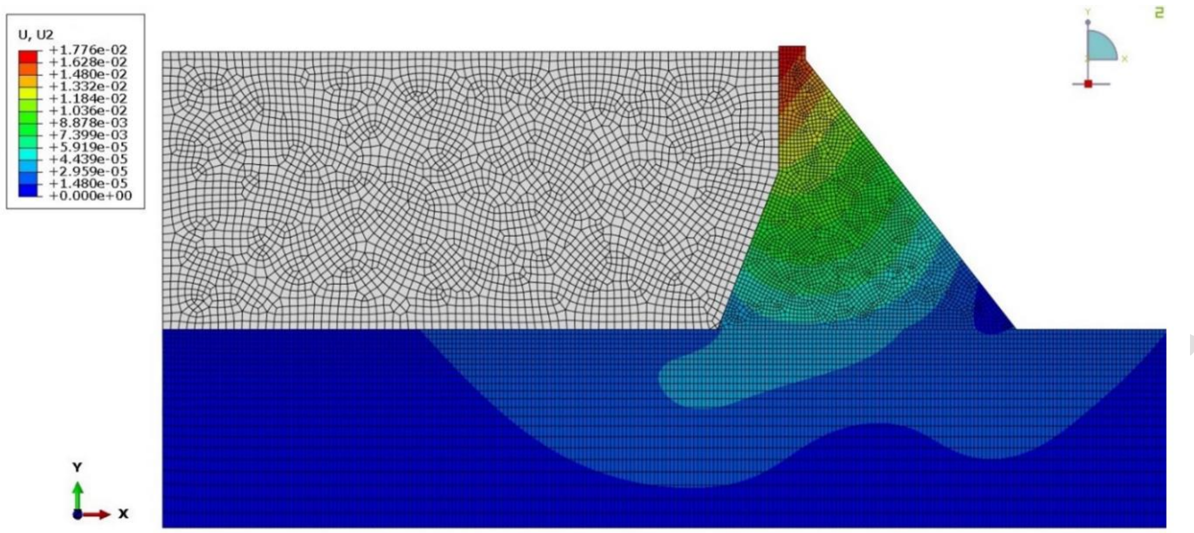

(c)

Figure 6. (a) Stress, (b) pore water pressure, and (c) displacement contours for the geostatic analysis step

The pore water pressure illustrated in Figure 7 shows a maximum pore water pressure of 0.057 MPa, which has reached a steady state, indicating that the soil conditions stabilized and the analysis time was adequate.

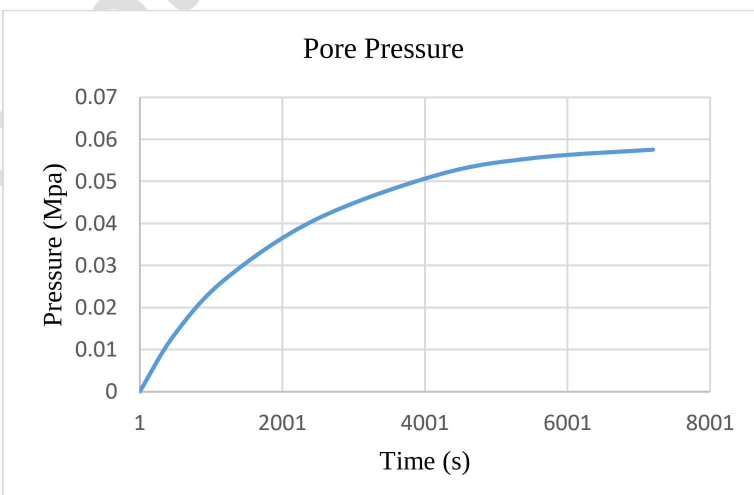

Figure 7. Pore water pressure at the heel of the dam during the soil analysis step

Figure 8(a) presents the pore water pressure contours at the mid-point of the earthquake analysis step. The maximum pore water pressure of 0.057 MPa is observed beneath the concrete dam due to its self-weight and at the water dam interface in the lower part of the dam's body, caused by the water wave pressure. Conversely, Figure 8(8) shows the stress contours for the soil analysis step, indicating a maximum stress of 5.21 MPa at the geometric discontinuity of the dam, a known weak point in concrete dams.

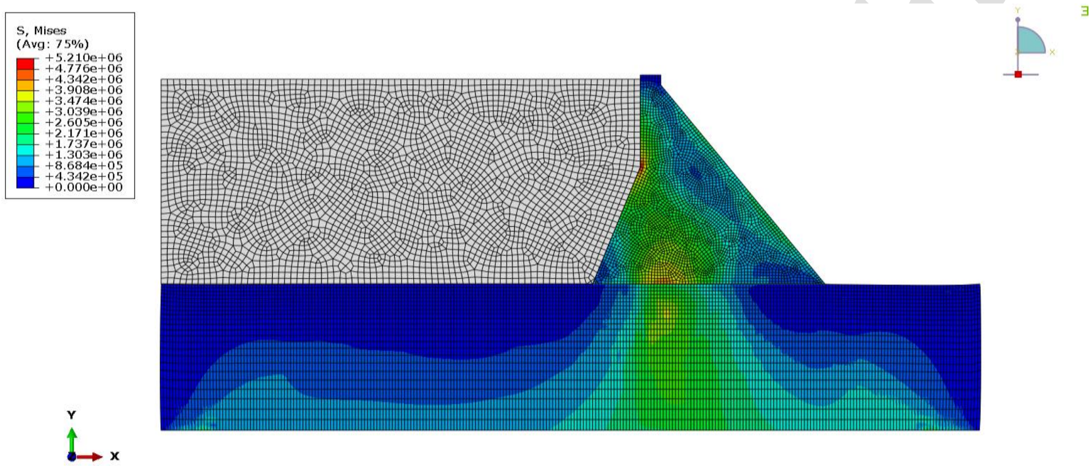

(a)

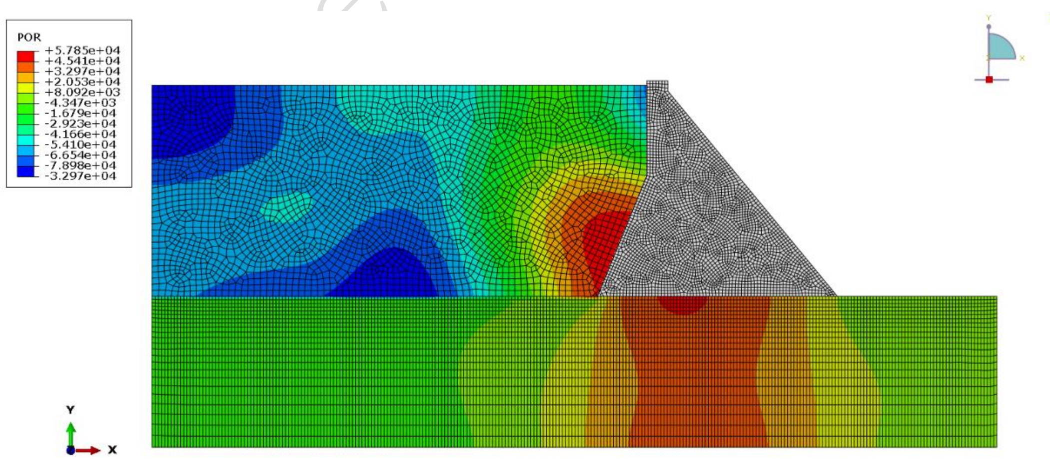

(b)

Figure 8. (a) Pore water pressure and (b) stress contours during the earthquake analysis step

Figure 8(a) depicts the chart of a water pressure contour sample at the midpoint of the seismic analysis step. According to this chart, the maximum water pressure is 0.057 MPa, occurring beneath the concrete dam due to the self-weight of the dam. Additionally, in the water reservoir, near the boundary between the dam and water, as well as in the lower half of the dam body, this pressure occurs due to wave formation in the reservoir. In contrast, Figure 8(b) depicts the stress contour chart during the soil analysis step. According to this chart, a maximum stress of 21.5 MPa occurs at the geometric fracture point of the dam, a location considered a weakness in concrete dams.

8.5 Morgan Hill Accelerogram Results

The Morgan Hill accelerogram results and their impact on the dam body are presented in this section. Figure 9 illustrates the development of cracks across the dam body during the earthquake over the applied time frame (Figure 2c), with the cracks beginning to propagate following the onset of the earthquake. According to Figure 2c, during the maximum applied acceleration of the earthquake at approximately the 10th second of the earthquake, the cracks reach their maximum extent and continue to propagate until the end of the earthquake. A detailed description of the cracks is as follows: The cracks initially appear at the dam face and gradually propagate from the geometric fracture point. Eventually, the cracks continuously expand between the face and the geometric fracture sections and affect larger sections of the dam. The analyses reveal that longitudinal damage also occurs at the heel of the dam, propagating along the distance between the heel and the toe. This phenomenon implies that the damage mechanisms caused by the earthquake initially occur in specific areas of the dam. The progression of the damage process and the gradual expansion of the cracks can also be observed in other sections of the dam body.

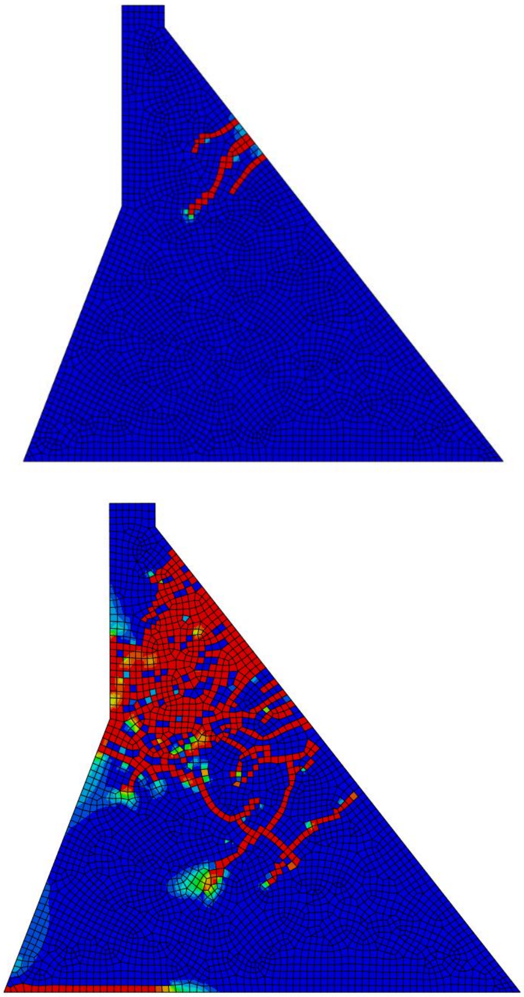

Figure 9. Crack propagation in the dam body during the earthquake event

Figure 10(a) depicts the lateral displacement graph of the dam crest during the earthquake up to a maximum value of 11 centimeters. This lateral displacement is mainly caused by the waves created by the reservoir and their impact on the dam walls. These waves transfer the energy of the earthquake to the dam structure through the reservoir, leading to its tendency to tilt downstream, which manifests as the previously stated displacement.

Figure 10(b) depicts the vertical displacement graph of the dam crest up to a maximum value of 3.5 centimeters. This vertical displacement represents the settlement at the dam crest, showcasing the earthquake's impact on the dam structure. The settlement of the dam crest represents the degree of deviation in the dam structure from its original position during the earthquake and its susceptibility to the vertical forces of the earthquake.

Additionally, Figure 10(c) shows the pore water pressure variation at the dam base (i.e., heel-to-toe) during the earthquake. The maximum pore water pressure is 0.065 MPa. However, these variations are closely related to the vertical displacement of the dam and the pressure changes in the soil. As shown in the Figure, the pore pressure gradually increases and oscillates around 0.06 MPa. This clearly indicates that the pore water pressure is influenced by the settlement of the dam; as the settlement increases, the stresses in the soil also rise, causing the pore water pressure to increase accordingly.

The pore water pressure exhibits relatively small variations over time during the earthquake. Nevertheless, these variations are closely linked to the vertical displacement of the dam and the pressure changes in the soil. As presented in the Figure, the pore water pressure gradually increases, fluctuating around 0.06 MPa. This is a clear indication that dam settlement significantly impacts pore water pressure. Consequently, with the settlement increase, the stresses within the soil also rise, leading to pore water pressure to increase.

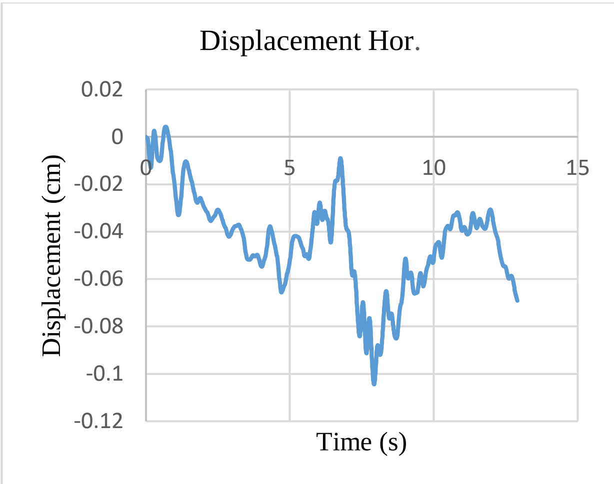

(a)

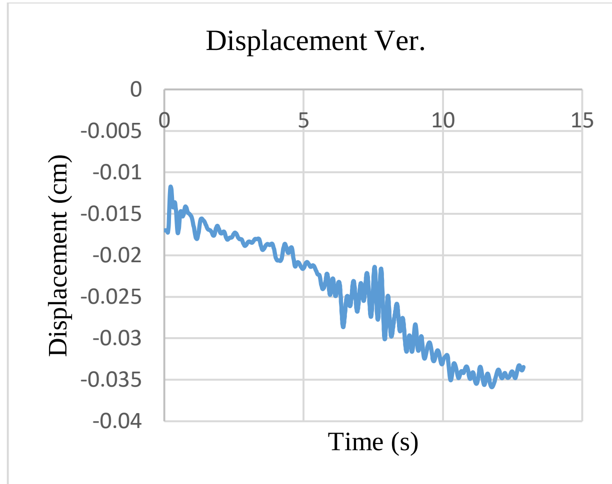

(b)

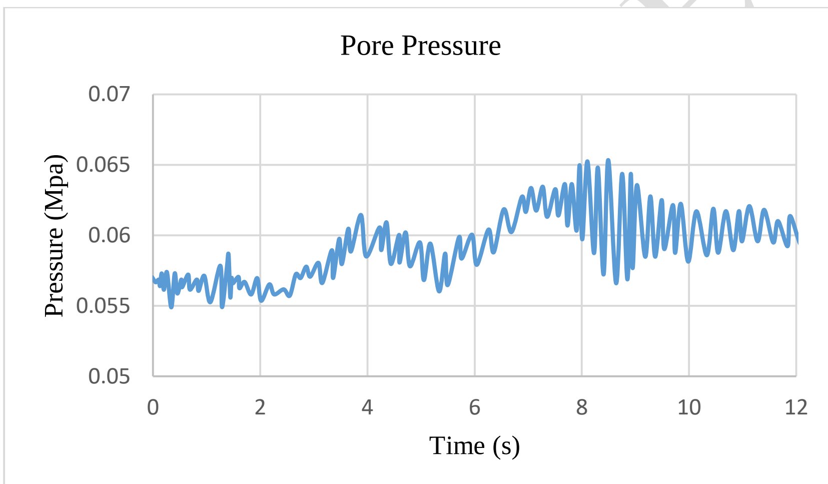

(c)

Figure 10. (a) Vertical displacement of the crest, (b) horizontal displacement of the crest, and (c) pore water pressure at the base during the earthquake event

8.6 Northridge Accelerogram Results

Figure 11 illustrates the propagation of cracks in the dam body during the earthquake over the applied time frame (Figure 2b), with the cracks beginning to propagate in response to the increased intensity of the vibrations following the onset of the earthquake. With the rise in amplitude of the vibrations, corresponding to the turning point in Figure 2b, which occurs approximately at the 8th second of the earthquake, the cracks reach their maximum extent. With the reduction of energy and the end of the earthquake, the crack propagation halts as well. A detailed description of the propagation of the cracks is as follows: The cracks initially appear in the face of the dam, where the cracking is mostly concentrated. The cracks gradually begin to grow from the geometric fracture point, eventually expanding between the face and the geometric fracture. The significant crack propagations in the face of the dam in this stage represent the centration of earthquake stresses in this area. The crack propagation rate in the face of the dam represents the structural weakness of this dam section and its sensitivity to applied stresses.

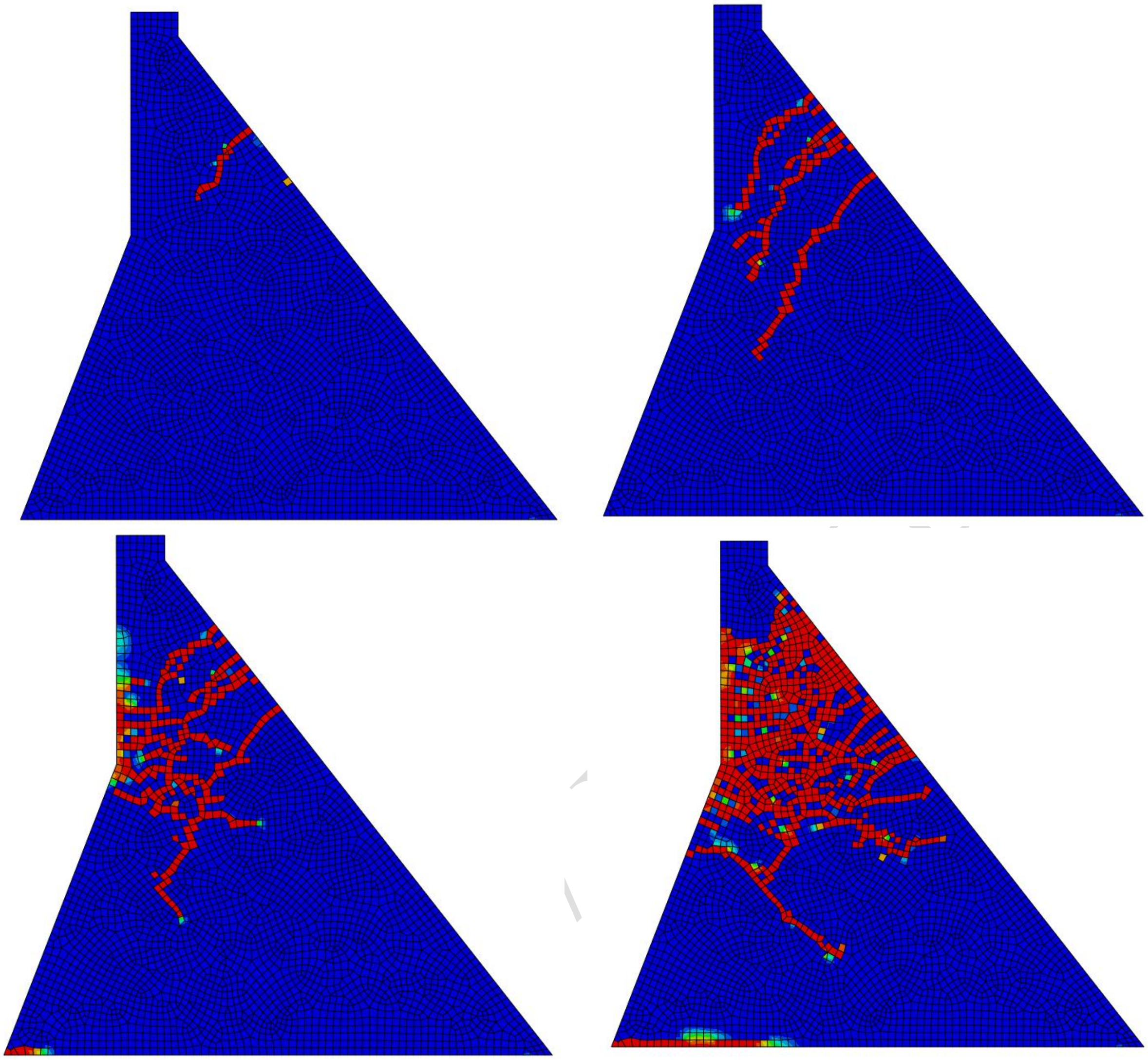

Figure 11. Crack propagation in the dam body during the earthquake event

Figure 12(a) depicts the graph of the lateral displacement of the dam crest during the earthquake up to a maximum of 8.69 cm. This amount of displacement indicates that the dam crest has shown a tendency to tilt downstream due to the waves generated during the earthquake.

Figure 12(b) depicts the graph of the vertical displacement of the dam crest during the earthquake up to a maximum of 8.69 cm. This displacement represents the displacement in the dam crest. This settlement is a damage indicator and reflects the deviation of the dam from its original position under the vertical stresses induced by the earthquake.

Figure 12(c) depicts the graph of the pore water pressure change downstream section of the dam (between the heel and the toe) during the earthquake. According to this graph, the maximum pore water pressure is 0.064 MPa. Although the pore water pressure undergoes relatively small variations during the earthquake, the variations are influenced by the vertical displacement of the dam and are closely linked to the internal pressures in the soil. Pore water pressure fluctuates based on the settlement of the dam crest and changes in soil pressure, with an increase in dam settlement impacting pore water pressure and leading to its relative rise.

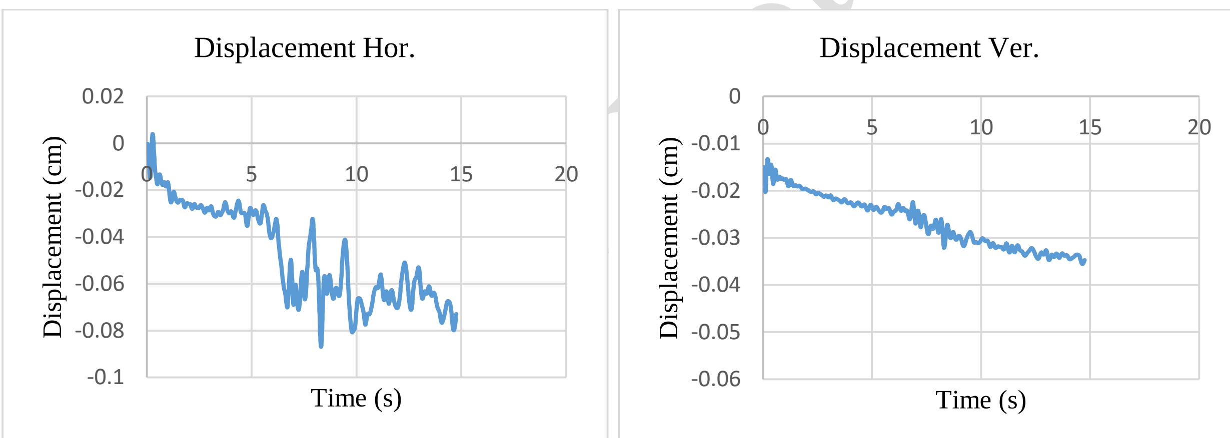

(a) (b)

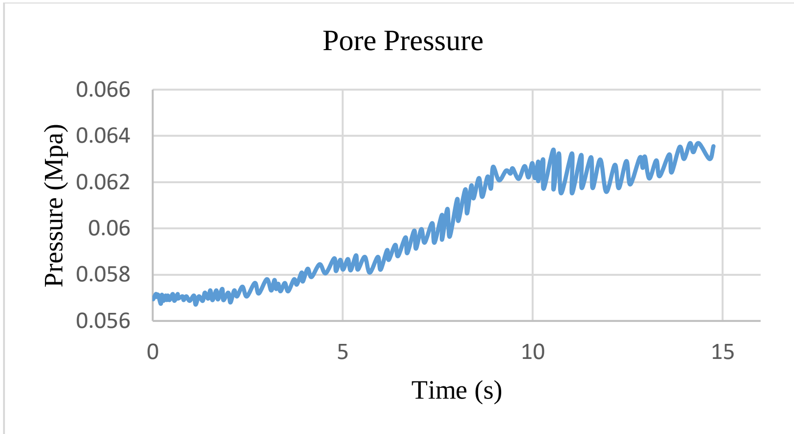

(c)

Figure 12. Dam response graphs during the earthquake

a) Lateral displacement of the dam crest b) Vertical displacement of the dam crest c) Pore water pressure change at the bottom of the dam

8.7 Loma Prieta Accelerogram Results

In this section, the results from the analysis of the Loma Prieta accelerogram and their impact on the structural behavior and stability of the studied dam are discussed. The resulting charts indicate the existence of structural changes and crack propagations in different dam sections. Figure 13 illustrates the development of cracks in the dam body during the earthquake over the seismic acceleration application time (Figure 2a), with the cracks beginning to propagate following the onset of the earthquake. According to Figure 2a, during the maximum applied acceleration of the earthquake at approximately the 10th second of the earthquake, the cracks reach their maximum extent. Finally, with the gradual reduction of the earthquake energy and the decrease in fluctuation amplitudes, the rate of crack propagation decreases and begins to advance until the final moment. A detailed description of the propagation of the cracks is as follows: The crack first occurs at the dam's upstream face, advancing at the area between the upstream face and the toe. This crack propagation is more pronounced in the midsection of the dam, with more extensive damage being observed in this area compared to other accelerogram records. The cracks in this section demonstrate more transverse propagation, with lower longitudinal propagation.

The lateral crack propagation pattern is clearly visible in the geometric fracture area, leading to an increase in crack width. In the heel area, the damage is largely tensile in nature and is distinct from the observed crack growth.

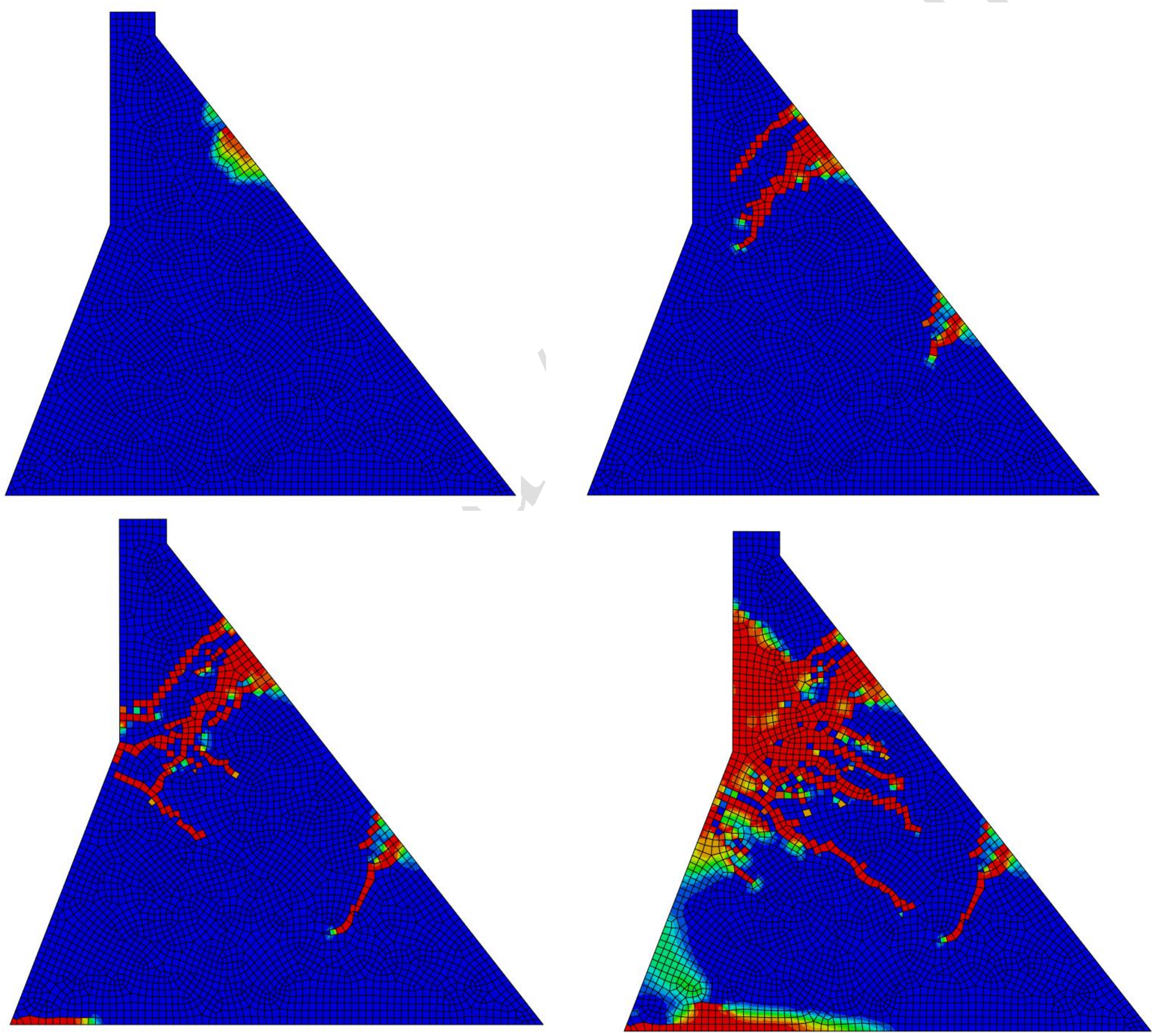

Figure 13. Crack propagation in the dam body during the earthquake

Figure 14(a) depicts the graph of the lateral displacement of the dam crest during the earthquake, reaching a maximum of 8.2 cm, which signifies significant changes within this area. Figure 12(b) depicts the graph of the vertical displacement of the dam crest during the earthquake up to a maximum of 3.1 cm. This indicates the occurrence of that settlement in the dam during the earthquake.

Additionally, Figure 14(c) depicts the graph of the pore water pressure change at the bottom of the dam (between the heel and the toe) during the earthquake. According to this graph, the maximum pore water pressure has reached 0.064 MPa, with relatively minor variations throughout the earthquake. However, these pressure changes are correlated with the vertical displacement of the dam and are influenced by soil pressure variations. Overall, these analyses indicate that the gradual settlement of the dam during the earthquake has resulted in an increase in pore pressure within a range of approximately 0.06 MPa.

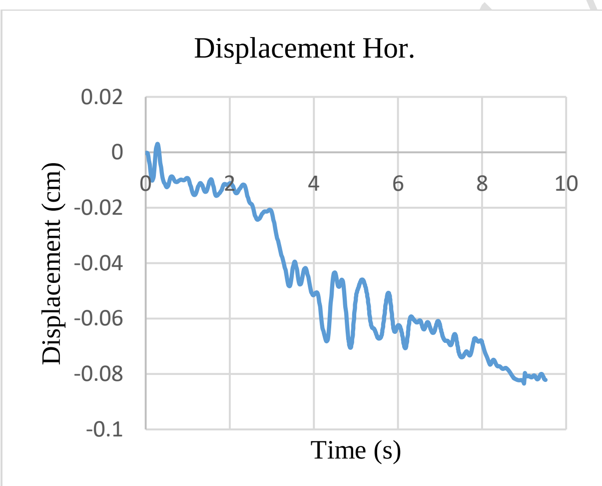

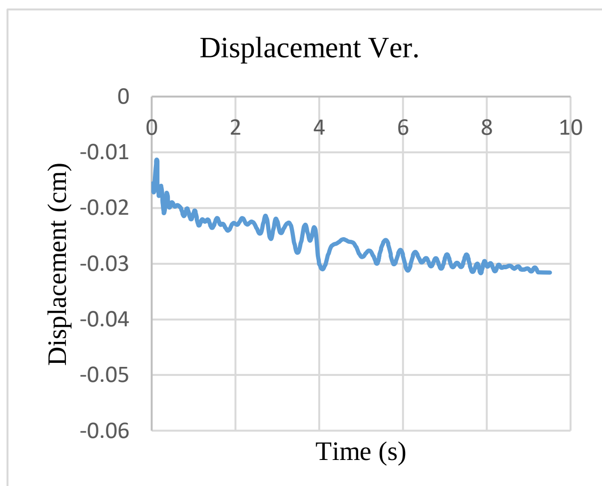

(a)

(b)

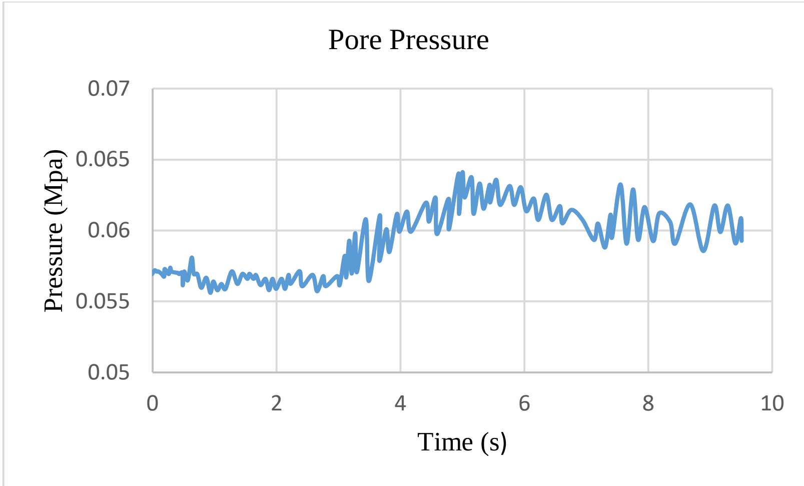

(c)

Figure 14. Dam response graphs during the earthquake

a) Lateral displacement of the dam crest b) Vertical displacement of the dam crest c) Pore water pressure change at the bottom of the dam

8.8 Results Comparison

As shown below, the various accelerogram records will now be compared based on the outcomes of the analyses done on the data. In the case of the crest lateral displacement of the dam during the earthquake, the comparative graph is shown in Figure (15) along with the selected three seismic records. Regarding this graph, the maximum lateral displacement of the dam's crest is 11 cm, corresponding to the Morgan Hill accelerogram record. This record is also associated with the maximum relative changes.

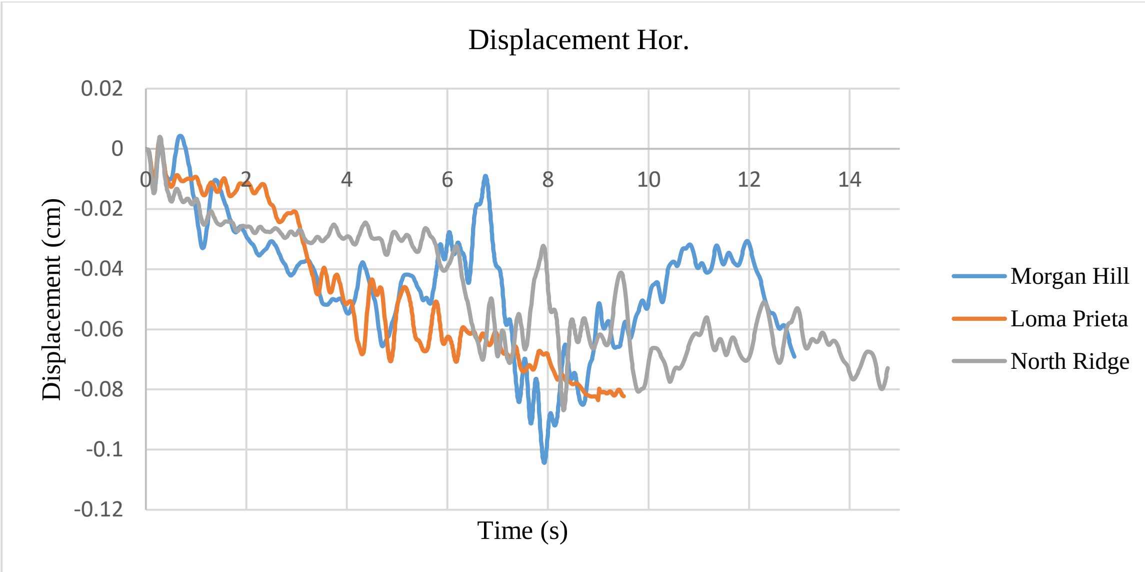

Figure 15. Comparative graph of the lateral displacement of the dam crest during the earthquake

Table (3) shows the comparison of the horizontal displacement results of the present study and the paper by Kalateh and Ghamatloo (Kalateh & Ghamatloo, 2018), taking into account the uplift force. The difference is that in the said study the uplift force was applied as a constant trapezoidal load, but in the present study, considering the pore water pressure as a variable during the analysis, the uplift force was calculated computationally through the software itself and applied at each moment, and is actually a function of the instantaneous pore water pressure conditions in the model during the seismic record.

Table (3): Comparison of horizontal displacement results of the present study and the study by (Kalate and Ghamatlo, 2018)

Seismic Record	**Horizontal Displacement**	
	Present Study	Kalateh & Ghamatloo, 2018
Loma Prieta	7.5 cm	8.2 cm
Northridge	8.4 cm	8.69 cm
Morgan Hill	9.6 cm	9.73 cm

Figure (16) shows the comparative graph of the vertical displacement of the dam crest during the earthquake based on 3 selected accelerogram records. According to this graph, the maximum vertical displacement of the dam crest is related to the Northridge accelerogram record with a value of 4 cm. The minimum value is also related to the Loma Prieta accelerogram record with a value of 3 cm. Also, Figure (17) shows the comparative graph of the pore water pressure during the earthquake (between the heel and toe) based on 3 selected accelerogram records. According to this graph, the maximum pore water pressure is related to the Morgan Hill accelerogram record with a value of 0.065 MPa. The maximum pore water pressure for the other two seismic records is around 0.064. According to this graph, the changes in pore water pressure generally have high oscillations with a relatively small amplitude during the earthquake.

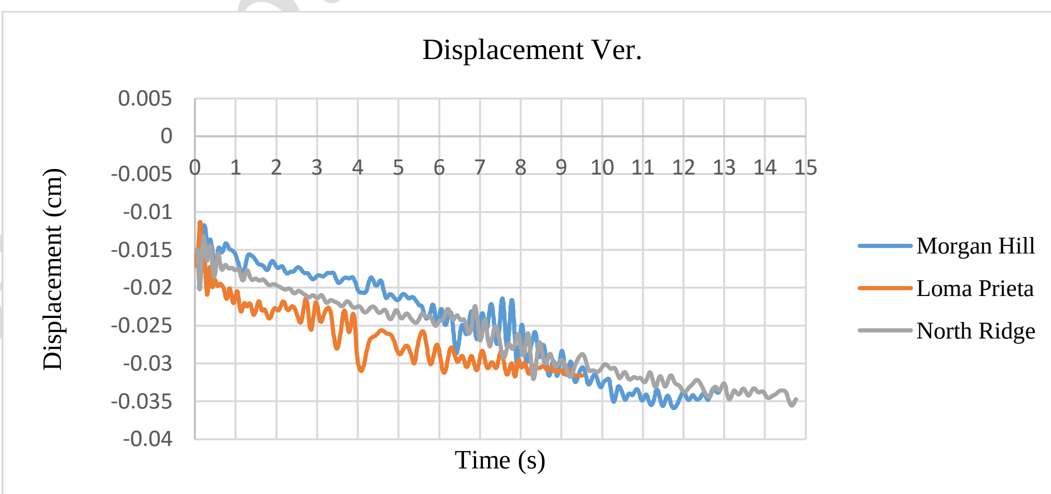

Figure 16. Comparative graph of the lateral displacement of the dam crest during the earthquake

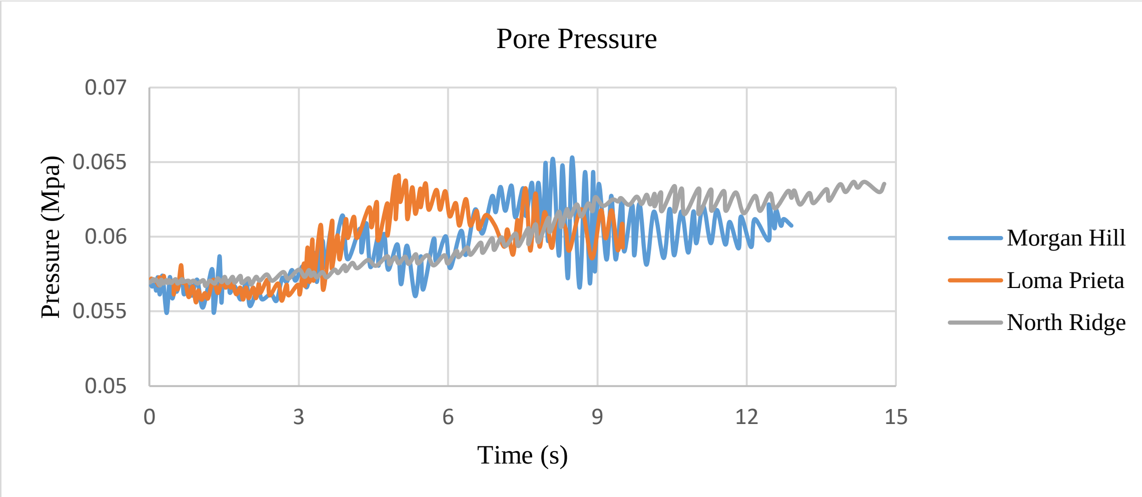

Figure 17. Comparative graph of the pore water pressure during the earthquake

9. Conclusion

Today, the issue of dam strength and stability is one of the most important topics of water management. Considering the high costs of dam construction and maintenance, the study and evaluation of the factors impacting dam strength and durability are sensitive, particularly under specific or undesirable conditions, are important. Uplift pressure on the dam structure is a critical issue in this context. Uplift pressure induced by water inside the cracks and pores of the dam can have a large effect on the mechanical behavior and overall stability of the structure. The dam structure is threatened by a potential adverse increase in uplift pressure and the potential for failure. This is a particularly important problem during earthquakes, as dams are subjected to sudden, extreme, or even critical loadings that can greatly enhance the effect of uplift pressure. In this study, the effect of uplift pressure distribution on the dam surface is analyzed, and the effect of seismic acceleration on concrete dams is investigated. Precise simulations and data from previous similar studies have been used to try to accurately evaluate the susceptibility of dam structures in crack areas under seismic loadings. The objective of this study was to identify potential weak points, crack propagation patterns, and damage in concrete dams during earthquakes.

The strengths of this study include accounting for the pore water pressure as a variable throughout the analysis, the interaction between the dam, reservoir, and foundation, and the analysis under various earthquake conditions. Conversely, the limitations of the study include the usage of two-dimensional modeling, failing to account for temperature and humidity variations, and the omission of foreshocks and aftershocks.

As a suggestion for a more detailed examination of the cracks, and given that the impact of pore water pressure on the displacement of the dam body and the propagation of cracks has been applied in this study, a three-dimensional analysis should be employed. This would allow for the incorporation of lateral forces across the entire dam volume (making pressure distribution appear more realistic), the possibility of examining how cracks propagate along the length of the dam (aiding in more realistic modeling of structural failure), and an improved analysis of localized water flow-induced erosion at various points in the dam.

The specific findings of this study are as follows:

1- Applying varying uplift forces beneath the dam necessitates the consideration of a set of impactful factors affecting the structural and mechanical behavior of the dam. These factors include pore water pressure, soil saturation percentage, and soil porosity. The geostatic forces of the soil and the gravitational forces applied from the reservoir and the dam to the soil, as well as the time required for the stabilization of the soil and the pore water pressure, should also be considered. For this purpose, ABAQUS is utilized to apply the accelerogram results and accurately simulate pore water pressure during the earthquake.

2- The earthquake generated waves in the dam reservoir that hit the dam and prevented the dam from returning to the reservoir and also generated a force that pushed the dam downstream. It may result in unexpected changes in the lateral displacement pattern of the dam. This study indicates that this lateral displacement is caused by earthquake-induced waves within the dam reservoir and has led to the dam tilting downstream. This is a critical change that can have a significant impact on dam stability and safety.

3- The vibrations caused by the earthquake apply forces on dam structures and gradually cause soil settlement beneath the dam. These vibrations penetrate deep within the soil and compress the lower layers, lowering their initial strength. Consequently, the concrete dam structure experiences changes, gradually tilting towards settlement.

4- The crack growth in all three accelerograms starts from the face and then starts to propagate at the point on the opposite side, the location of the dam's geometric failure. The dam structure experiences geometric changes at this point where crack propagation accelerates, and cracks at both sides of the area between the dam face and the geometric failure point experience significant tensile damages.

5- The pore water pressure experiences severe fluctuations in a small amplitude during the earthquake, leading to its limited direct impact on the lateral and vertical displacements of the structure. However, applying the actual uplift force distribution, as conducted in this study, leads to a relative increase in the lateral and vertical displacements of the dam compared to the conventional calculation methods and the manual application of the force in a trapezoidal form.

Although this relative increase is small, it is insignificant as even minor changes can gradually impact the dam's stability during seismic analysis. Additionally, these changes can create different or larger effects by expanding this study and research to other types of dams (earthen, arch, etc.) as well as other accelerograms or soils and foundations with different materials.

6- A comparison of the lateral displacement of the dam crest from the three selected accelerograms showed that the maximum lateral displacement of the dam crest during the earthquake belonged to the Morgan Hill accelerogram with a value of 11 cm. This accelerogram recorded the greatest displacement and most relative variations.

7- Analyzing the variation of the dam's crest by the vertical displacement during the earthquake depending on the selected three accelerograms, it is specified that under the action of the Northridge accelerogram, the maximum vertical displacement of the dam's crest is 4 cm only. In contrast, the lowest vertical displacement was observed in the Loma Prieta accelerogram, with a value of 3 cm. This variation in vertical displacement between the accelerograms illustrates the differences in loading patterns of each accelerogram on the dam structure.

8- The pore water pressure during the earthquake (between the heel and toe) for three selected records was compared. It was noted that the maximum pore water pressure depends on the Morgan Hill seismic record and is equal to 0.065 MPa. The pore water pressure is around 0.064 KPa at the maximum for the other two seismic records. The pore water pressure shows that the changes are frequent and have small oscillations during the earthquake, as shown in this graph.

References

Altunisik, A. C., Sesli, H., Hüsem, M., & Akkoşe, M. (2019). Performance evaluation of gravity dams subjected to near- and far-fault ground motion using Euler approaches. Iranian Journal of Science and Technology Transactions of Civil Engineering, 43, 297–325. https://doi.org/10.1007/s40996-018-0142-z

Arici, Y., & Soysal, B. F. (2024). Predicting seismic damage on concrete gravity dams: A review. Structure and Infrastructure Engineering, 20(9), 1354–1373. https://doi.org/10.1080/15732479.2022.2141270

Bolt, B.A. (2003) *Earthquakes* (5th edn). New York: W. H. Freeman. ISBN 0-7167-5618-8. https://doi.org/10.1007/s10950-005-2110-x

Eguchi, R.T., Goltz, J.D., Taylor, C.E., Chang, S.E., Flores, P.J., Johnson, L.A., Seligson, H.A., and Blais, N.C. (1998) 'Direct economic losses in the Northridge earthquake: A three-year post-event perspective', *Earthquake Spectra*, 14(2), pp. 245–264. https://doi.org/10.1193/1.1585998

Fang, W., He, J., Yu, Y., Hao, R., & Guo, Y. (2024). Numerical analysis calculations of ductile concrete gravity dams under seismic action. In Zheng, S., Taylor, R. M., Wu, W., Nilsen, B., & Zhao, G. (Eds.), Hydropower and Renewable Energies (Vol. 487). Lecture Notes in Civil Engineering. https://doi.org/10.1007/978-981-97-9184-2_3

Ghallab, A. (2020). Simulation of cracking in high concrete gravity dam using the extended finite elements by ABAQUS. American Journal of Mechanics and Applications, 8(1), 7–15. https://doi.org/10.11648/j.ajma.20200801.12

Gorai, S. M., & D., S. (2021). Seismic behavior of dams to near-fault and far-fault ground motions: A state-of-the-art review. Journal of Earthquakes and Structures, 21(3), 251–263.

Hajivand Dastgerdi, R., Shokati Beyrag, B., Kazemi, K., & Malinowska, A. (2022). Improving seismic performance of concrete gravity dams considering hydrodynamic effect and soil-structure interaction. International Journal of Engineering Research & Technology, 11(9).

Hussein, S., Kadir, T., Ramli, M. A. A., & M. Z. (2024). Numerical investigation of seismic load analysis for a concrete gravity dam utilizing ABAQUS software. Journal of Electrical Systems, 20(4s), 818–831. https://doi.org/10.52783/jes.2119

Joses Sorilla, Timothy Scott C. Chu, and Alvin Y. Chua (2024) 'A UAV Based Concrete Crack Detection and Segmentation Using 2-Stage Convolutional Network with Transfer Learning', *HighTech and Innovation Journal*, 5(3). https://doi.org/10.28991/hij-2024-05-03-010

Kalateh, F., & Ghamatloo, A. (2016). Comparison of massed and non-massed foundation on nonlinear dynamic response of weighted concrete dam in terms of dam-reservoir-foundation interaction. International Conference on Civil Engineering, Architecture, and Urban Planning of Contemporary Iran, Shahid Beheshti University.

Kalateh, F., & Ghamatloo, A. (2018). Investigating the effect of uplift on the seismic damage of weighted concrete dam in earthquakes in far and near areas. Journal of Structural and Construction Engineering, 6(1), 202–221. https://doi.org/10.22065/jsce.2017.93011.1271

Lee, J., & Fenves, G. L. (1998). Plastic-damage model for cyclic loading of concrete structures. Journal of Engineering Mechanics, 124(8), 892–900. https://doi.org/10.1061/(asce)0733-9399(1998)124:8(892)

Lubliner, J., Oliver, J., Oller, S., & Oñate, E. (1989). A plastic-damage model for concrete. International Journal of Solids and Structures, 25(3), 299–326. https://doi.org/10.1016/0020-7683(89)90050-4

Machelski, C., & Korusiewicz, L. (2021). Contact interaction between corrugated steel shell and the soil backfill determined based on the measurements of shell deformations. Journal of Archives of Civil Engineering, 67(1), 57–79. https://doi.org/10.24425/ace.2021.136461

Motallebiyan, A., Bayat, M., & Nadi, B. (2020). Analyzing the effects of soil-structure interactions on the static response of onshore wind turbine foundations using finite element method. Civil Engineering Infrastructures Journal, 53(1), 189–205.

Navaeinia, B., Naseri, N., Kalani, L., & Vathaghi Amiri, J. (2013). Evaluation of nonlinear response of weighted concrete dams with rotational and static crack modeling. First National Conference on Structural Engineering of Iran, Olympics Hotel Conference Center, Tehran, Iran.

Parvathi, I. S., Mahesh, M., & Kamal, D. V. V. R. (2022). XFEM method for crack propagation in concrete gravity dams. Journal of Institution of Engineers (India): Series A, 103, 677–687. https://doi.org/10.1007/s40030-022-00636-2

Praštalo, P., Uljarević, M., and Vukomanović, R. (2024) 'Effect of Breach Parameters and Progression Curves on Dam Failure Hydrograph', *Civil Engineering Journal*, 10(2). https://doi.org/10.28991/cej-2024-010-02-08.

Pundrik, P., Bahuguna, A., & Firoj, M. (2020). Near-fault and far-fault seismic analysis of concrete gravity dam. Journal of Hydraulic Structures, 6(2), 56–79.

Rahmati-Alaei, A., & Rokhy, H. (2025). Wave-Structure Interaction (WSI) Analysis for Dam Break with Dike using SPH and ALE Methods. Civil Engineering Infrastructures Journal. https://doi.org/10.22059/ceij.2025.383343.2167

Saksala, T., & Mäkinen, J. (2020). Numerical modelling of cracking in gravity dam under static and seismic loadings with multiple pre-embedded discontinuity FEM. Procedia Structural Integrity, 28, 784–789. https://doi.org/10.1016/j.prostr.2020.10.091

Sharma, A., & Nallasivam, K. (2023). Static analysis of a concrete gravity dam using the finite element technique. Asian Journal of Civil Engineering, 24, 2939–2957. https://doi.org/10.1007/s42107-023-00686-2

Sherong, G. (2013). Effects of near-fault and far-fault ground motions on nonlinear dynamic response and seismic damage of concrete gravity dam. Journal of Soil Dynamics and Earthquake Engineering, 53(1), 217–229. https://doi.org/10.1016/j.soildyn.2013.07.014

Tidke, A. R., & Adhikary, S. (2021). Seismic fragility analysis of the Koyna gravity dam with layered rock foundation considering tensile crack failure. Engineering Failure Analysis, 125, 105361. https://doi.org/10.1016/j.engfailanal.2021.105361

Toppozada, T.R., Real, C.R., and Parke, D.L. (1988) 'Preparation of isoseismal maps and summaries of reported effects for pre-1900 California earthquakes', *California Division of Mines and Geology*, Open-File Report 88-13, pp. 1–912. https://doi.org/10.3133/ofr81262

Tuswan, T., Muhammad, R., Prabowo, A. R., Yaningsih, I., Wibowo, W., Muttaqie, T., & Istanto, I. (2024). Seismic behavior of dams. EVERGREEN Joint Journal of Novel Carbon Resource Sciences & Green Asia Strategy, 11(3), 2217–2233. https://doi.org/10.5109/7236865

Wang, G., Lu, W., & Zhang, S. (2021). Seismic cracking analysis of concrete gravity dams with initial cracks using XFEM. In Seismic Performance Analysis of Concrete Gravity Dams (Vol. 57, pp. 53–77). Advanced Topics in Science and Technology in China. https://doi.org/10.1007/978-981-15-6194-8_3

Wang, M., Chen, J., Wei, H., Song, B., & Xiao, W. (2019). Investigation on seismic damage model test of a high concrete gravity dam based on application of FBG strain sensor. Complexity, 2019, 7837836. https://doi.org/10.1155/2019/7837836

Wang, Y. J., Wu, Z. M., Qu, F. M., & Zhang, W. (2022). Numerical investigation on crack propagation process of concrete gravity dams under static and dynamic loads with in-crack reservoir pressure. Theoretical and Applied Fracture Mechanics, 117, 103221. https://doi.org/10.1016/j.tafmec.2021.103221

Westergaard, H. M. (1933). Water pressure on dam during earthquakes. Transactions of the American Society of Civil Engineers, 98, 1303–1318. https://doi.org/10.1061/taceat.0004496

Yang, D., & Zhou, J. (2015). A stochastic model and synthesis for near-fault impulsive ground motions. Earthquake Engineering and Structural Dynamics, 44(1), 243–264. https://doi.org/10.1002/eqe.2468